Title
Statistical Analysis of Small-Scale Membrane Signaling Reactions: the Role of Membrane Recruitment and Catalysis

Author
Huang, Yuan-Chi

Publication Date
2016

Peer reviewed|Thesis/dissertation

Statistical Analysis of Small-Scale Membrane Signaling Reactions: the Role of Membrane Recruitment and Catalysis

By

Yuan-Chi Huang

A dissertation submitted in partial satisfaction of the

requirements for the degree of

Doctor of Philosophy

in

Chemistry

in the

Graduate Division

of the

University of California, Berkeley

Committee in charge:

Professor Jay T. Groves, Chair
Professor John Kuriyan
Professor Ahmet Yildiz

Fall 2016

Abstract

Statistical Analysis of Small-Scale Membrane Signaling Reactions:

the Role of Membrane Recruitment and Catalysis

by

Yuan-Chi Huang

Doctor of Philosophy in Chemistry

University of California, Berkeley

Professor Jay T. Groves, Chair

Molecular kinetics in living systems fundamentally shape the response function of signal transduction. Signaling cascades in cells are often initiated and amplified at the plasma membranes, where decisions are made under constant presence of molecular noise. Conceivably, the signaling geometry of membrane reactions are intimately related to the system's ability to robustly detect signals, down to single-molecule level. However, the physical mechanisms of signal transduction embedded in membrane signaling reactions are poorly understood. One of the limitations stems from a lack of well-controlled experimental assay to conceptualize the role of stochastic processes in membrane signaling. In this dissertation, I attempt to lessen this gap by developing single-molecule assays accompanied with statistical kinetics theory to analyze the molecular processes of reconstituted biochemical systems, derived from T-cell receptor triggering, on supported membranes. Broadly speaking, cytosolic proteins in membrane signaling reactions commonly follow a membrane recruitment-activation protocol. Therefore, the content of this dissertation will begin by discussing the role of membrane recruitment in signaling accuracy, with specific emphasis on kinetic proofreading. The later section focuses on the activities after successful activation, from determination of simple catalysis to elaboration of a bistable network response. These discourse hopefully provide a basis to discuss the design principles underlying signaling reactions.

Table of Contents

Acknowledgement

In my modest opinion, I believe that when one actually accomplishes something, one should remember that there are always luck. Luck comes in various forms, one of them is being surrounded by highly intellectual and talented as well as unconditionally supportive individuals.

First of all, I thank my Ph.D. advisor, Prof. Jay Groves. His intellectual guidance and training for me is without questioning. Yet I am especially grateful for the abundant opportunities, academic freedom and encouragement he provided. As Napoleon once said, "ability has nothing to do with opportunity." It is extremely fortunate for a young scholar to immerse in this environment.

Next, I thank the entire lab from the past to presence for both direct and indirect contribution. I am especially grateful to be trained by talented postdoctoral fellows and senior graduate students, including Dr. Wan-Chen Lin, Dr. Hsiung-Lin Tu, Dr. Sune Christensen, Dr. Lars Iversen, Dr. Christopher Rhodes, Dr. Hector Huang, Dr. Il Hyung Lee and Dr. Michael Cole. My current colleagues help tremendously in realizing the projects, including Dr. Jean Chung, Dr. Scott Hansen, Dr. Young Kwang Lee, Steven Alvarez, Dr. Shalini Now-Lam, Jenny Lin, Monatrice Lam, and Han-Kuei Chiang.

I am also grateful to have interacted with many experts in the field, including Prof. John Kuriyan, Dr. Qingrong Yan, Dr. Neel Shah, Dr. Yasushi Kondo, Dr. Julie Zorn, Prof. Michael Rosen, Dr. Jonathan Ditlev, Prof. Ronald Vale, Dr. Xiaolei Su, and Dr. Enfu Hui. I sincerely believe that active collaboration is an integral part of modern physical bioscience.

I thank my dissertation committee, Prof. Ahmet Yildiz, for his feedbacks. I also thank Prof. Phillip Geissler for the rigorous theoretical training. Furthermore, I thank all my mentors in the past, who guided me to where I am now.

Lastly, I thank my family for their unconditional support. Their support are always beyond what words can describe. My significant other as well as friends are also important in making the journey mentally sustainable. For that, I thank all of them as well.

I deeply apologize if I missed any names. I am grateful and thankful for all the support I have throughout these years. With these in mind, I hope that I am always humble with my work.

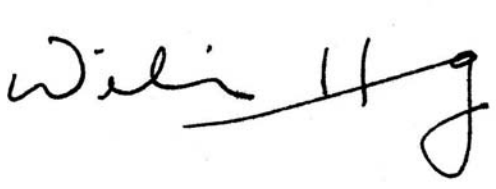

William Y. C. Huang
University of California, Berkeley
Nov. 16, 2016

Statistical Analysis of Small-Scale Membrane Signaling Reactions: the Role of Membrane Recruitment and Catalysis

William Y. C. Huang

1. Introduction

Signaling reactions are the fundamental building blocks of living systems. Through a cascade of chemical reactions, cells can detect target, make logical decision, and respond appropriately. All of which happen in a noisy, stochastic environment. The capability to perform robust signaling, down to single-molecule level, is of great interests, both physically and biologically. A common feature shared by many signaling reactions is that they operate and often initiate on membrane surfaces (2), e.g. T-cell receptor at the plasma membranes can detect a single agonist that triggers a series of phosphorylation events leading to recruitment of cytosolic proteins (3-6). Therefore, the response function at this interface must be able to proofread genuine signals from spontaneous molecular noise, for both extracellular recognition and intercellular trafficking. Although the molecular mechanism is poorly understood, it can be hypothesized that membranes facilitate the accuracy and efficiency of signal transduction. However, the only way to examine this unifying principle is to first understand how these reactions function at the molecular level.

This dissertation, with the title "*Statistical Analysis of Small-Scale Membrane Signaling Reactions: the Role of Membrane Recruitment and Catalysis*", focuses on discussing how signaling reactions in the cytoplasmic side of the plasma membranes achieve high precision in a stochastic environment, mechanistically. "Statistical analysis" is not at all emphasizing the mathematical framework of stochastic process, in fact all the calculations used are rudimentary. Rather, in many instances conceptualization of the signaling process is best demonstrated concretely by the statistical approach. "Small-scale membrane signaling reactions" is our focus. The emphasis of "small-scale" describes the length scale of interest (~1-100 protein copy number), which happens to be functional in living systems as well. "Membrane" will be the unifying theme that connects all the chapters: the observed dynamics uniquely happen on membranes, and absence in solution. While there are many facets of signal transduction on membranes to study, I focus on "the role of membrane recruitment and catalysis". The recurring pattern of membrane recruitment followed by activation and catalysis, a process I like to call membrane recruitment-activation protocol, describes many signaling reactions. This commonality inspires the hypothesis that membrane recruitment facilitate robust signaling in a noisy environment. While the bulk part of this dissertation focuses on studying how membrane signaling reactions exhibits high precision, hopefully it also provides evidences to discuss why – the underlying design principle of signal transduction.

To have a concrete system to discuss, I focus on reactions derived from T-cell receptor (TCR) signaling pathway (Fig. 1-1). TCR activation involves a well-documented spatiotemporal coordination of a multitude of membrane proteins, which orchestrate its capability to recognize agonist, store and amplify signals, and subsequent gene expression and T-cell regulation (3, 5, 7-9). TCR activation generally initiates with engagement of peptide major histocompatibility complex (pMHC) with TCR, leading to the recruitment of cytosolic kinase zeta-chain-associated protein kinase 70 (Zap70) and phosphorylation of membrane adaptor protein, linker of activation of T cell (LAT). This triggers phosphotyrosine-mediated molecular assemblies on membranes that recruits components from the cytosol, including growth factor receptor-bound protein 2 (Grb2) and Sons of Sevenless (SOS). SOS is a guanine nucleotide exchange factor (GEF) that catalyze nucleotide exchange in Ras. This cascade further leads to recruitment of rapidly accelerated fibrosarcoma kinase (Raf) and downstream extracellular signal–regulated kinases (Erk) phosphorylation, and gene expression. The commonality of membrane recruitment-activation protocol is evident from the signaling map.

Instead of following the conventional signaling pathway, this dissertation is sectioned according to the stochastic process itself (Fig. 1-1): membrane recruitments and catalysis on membranes. The first section focuses on membrane recruitment. Recruitment is not only stable localization of proteins on membranes, the process embed the ability to proofread genuine signal from molecular noise. The proofreading is achieved through the competitive kinetics of the molecular process, classically termed as kinetic proofreading by Hopfield in 1974. I will begin with the theoretical foundation of kinetic proofreading recast from the perspective of statistical kinetics, which will clarify the role of membrane dwell time in this mechanism (Ch. 2). Subsequently, experimental evidence of kinetic proofreading during membrane recruitment will be elaborated (Ch. 3). A physical mechanism of controlling kinetic proofreading – via molecular assembly - is next discussed (Ch. 4), along with characterization of the identity of the assembly structure. In the second section, I discuss catalysis on membranes, typically after successful recruitment and activation. Measurement of enzymatic reactions on membrane is often *ad hoc*, hence a general assay to quantify membrane enzymology is first discussed (Ch. 5). Next, the effect of molecular

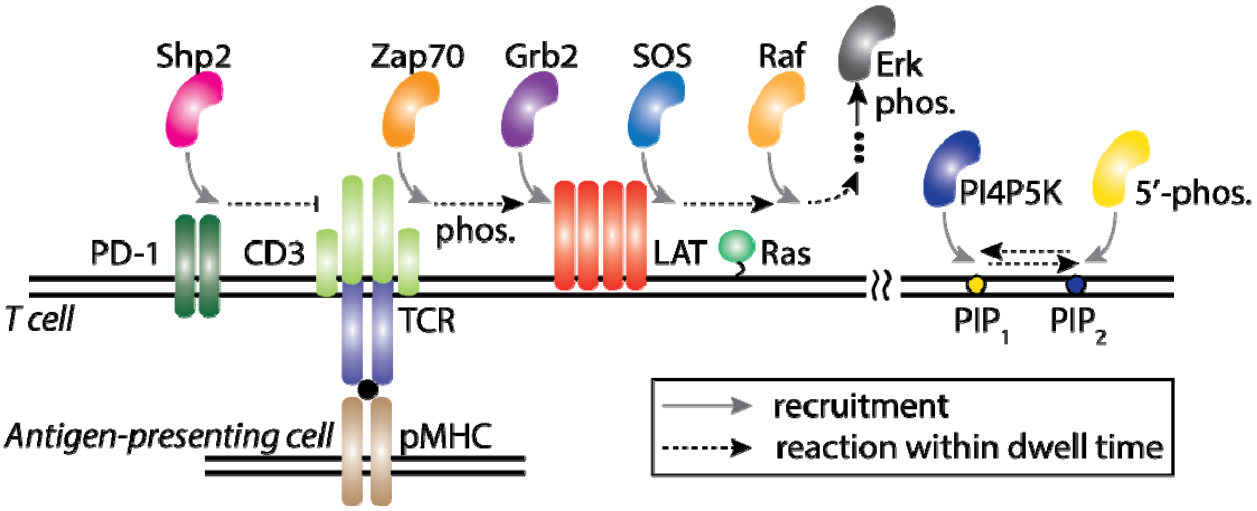

Fig. 1-1. Membrane signaling reactions in T-cell receptor activation pathway. Cytosolic enzymes typically follow a general activation protocol: membrane recruitment, followed by catalysis on membranes.

configurations on catalysis is briefly explored (Ch. 6). Finally, I end with an exotic property of competitive enzymatic reactions on membranes that can achieve geometry sensing (Ch. 7) – the product of the reactions depends on the system's size. This realization, driven by a complex mix of membrane recruitment and catalysis, give rise to bistability in system level response. Other than following the stochastic processes themselves, the dissertation progresses with increasing complexity of our observations, from single-molecule dynamics to small assembly structures to small signaling networks to outlook on cellular experiments. The future prospect to develop a framework connecting molecular processes and system level response inspired by these discourse will be hinted in the final chapter (Ch. 8).

Part I. Membrane recruitment

2. Kinetic proofreading in membrane recruitment: a statistical kinetics perspective

The molecular timing of how a signaling molecule activate fundamentally shaped the response function of a signaling cascade of a living system. In many salient examples, such as T-cell receptor (TCR) triggering, decision making of signal transduction are executed at the plasma membranes, where cytosolic proteins are recruited typically in response to modification of membrane receptors including phosphorylation (10). Many of these cytosolic enzymes, for instance Sons of Sevenless (SOS), have multidomain regulations that autoinhibit its activity in solution, and only activate on membranes after release of autoinhibition (11, 12). The requirement to release autoinhibtion in the activation pathway posits that activation on membranes is a multistep process involving a few kinetic intermediates rather than a single step process (12, 13). In other words, a finite time is required for the molecule to overcome the kinetic barriers and structurally reconfigure itself to activate. Therefore, the amount of time the molecule spent on membranes, i.e. membrane dwell times, is consequential to the probability of activation itself (13). And this discerning mechanism, classically known as kinetic proofreading (14), based on competing kinetics between activation and dissociation can filter molecular noise of different kinetics from genuine signals. However, these analysis are built upon understanding the distributions and statistics (15-19) of the activation profile of cytosolic enzymes on membranes, which are yet to be inspected experimentally.

From the single-molecule point of view[1] (16, 17), SOS (or any other cytosolic enzyme) can be defined to reach activation on the membrane at time t if: ***i***) it is still bound to the membrane at time t and, ***ii***) it advances through all kinetic intermediates at time t (Fig. 2-1A). Considering dissociation as a Poisson process parameterized by a rate constant k_{-1}, the probability density of activation on the membrane, $p(t)$, can be expressed as:

$$p(t) = e^{-k_{-1}t} \cdot p_N(t) \qquad [2.1]$$

[1] Contents beginning from this paragraph to the end of chapter 2 are published in Huang *et al. PNAS*, 2016, **113**:8218.

where $p_N(t)$ is the distribution of activation time for N kinetic intermediates. Progression through a series of N kinetic intermediates can be described as a series of Poisson processes, with kinetic rates $\{k_1, k_2, \ldots, k_N\}$, for the N intermediates, and k_A for the final activation step (Fig. 2-1A), such that $p_N(t)$ is the successive convolution of the lifetime probability distribution at each step:

$$p_N(t) = k_1 e^{-k_1 t} \otimes k_2 e^{-k_2 t} \otimes \ldots \otimes k_N e^{-k_N t} \otimes k_A e^{-k_A t} \quad [2.2]$$

Although the rate constants in this model are independent and can differ from each other, the qualitative features of $p_N(t)$ (e.g. shape of the distribution) are readily revealed in the simplifying case where individual kinetic transitions have equal rate constants, in which case $p_N(t)$ is a gamma distribution, $p_N(t) = \big((N+1)k_N\big)^{N+1} t^N e^{-(N+1)k_N t}/N!$ (Fig. 2-1B). Note that we consider a 1-parameter class of activation time distributions with constrained rate constants, i.e. transition rate constant $= (N+1)k_N$, such that the mean activation time remains identical regardless of N. This allows examination of the dependence of activation rate solely on the activation mechanism instead of the activation time. Integrating $p(t)$ yields the probability to activate for a single recruitment event, P_{act}. To calibrate the strength of a kinetic proofreading effects, we calculate the rate of activation, j_{act}, for a single molecule under stationary conditions:

$$j_{act} = \frac{P_{act}}{\langle \tau \rangle} = (N+1)k_A \frac{1-r}{1-r^{N+1}} r^N \quad [2.3]$$

where $r = (N+1)k_N/((N+1)k_N + k_{-1})$. This analysis is general and can describe the activation of other cytosolic enzymes on membranes.

The rate of SOS activation, j_{act}, is plotted in Fig. 2-1C as a function of the ratio of mean dwell time over mean transition time (k_N/k_{-1}). For $N = 0$, the rate of activation is identical regardless of the dwell time. In other words, when there are no kinetic intermediates en route to activation, the rate of SOS activation is proportional to the amount of membrane recruited SOS at any given time and does not depend on the dwell times for individual proteins. In this situation, kinetic proofreading is not possible. For $N > 0$, the activation rate decreases as dwell time decreases. This inequality in activation rate stems from the change in the distribution (not in the average) of the activation times, $p_N(t)$, when kinetic intermediates are involved (Fig. 2-1C). Physically, a short dwell time does not provide sufficient time for the enzyme to restructure and reach activation. Hence to achieve kinetic proofreading for the activation of cytosolic enzymes, two requirements must be met: ***i)*** elongation of dwell time and, ***ii)*** a multistep activation.

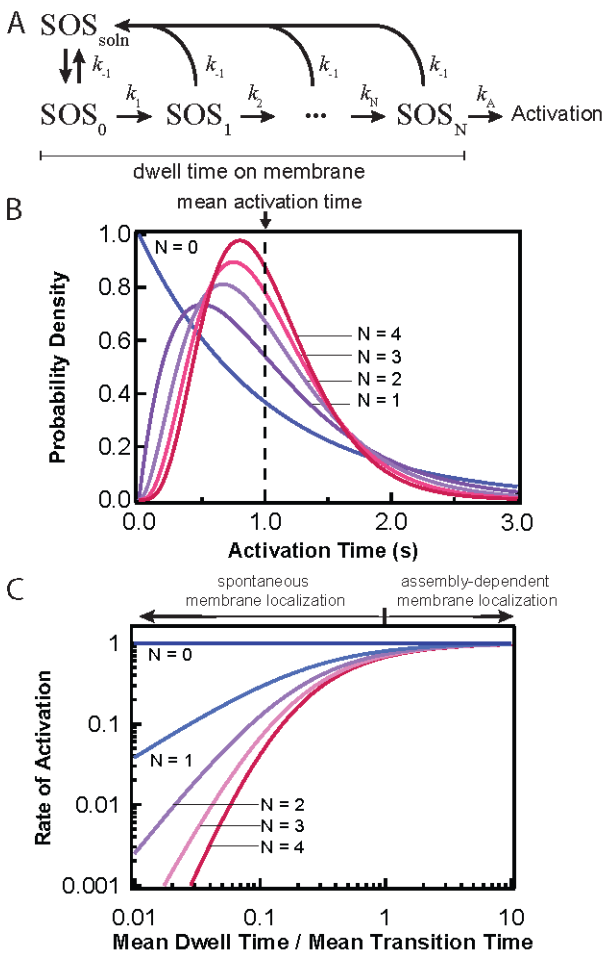

Fig. 2-1 Mechanistic requirements for kinetic proofreading of SOS activation on membranes. (A) Kinetic model for SOS activation. Following membrane recruitment of SOS, conformational transitions are required to release auto-inhibition. The subscript for SOS denotes the kinetic intermediates, where N is the total number of kinetic intermediates preceding activation. k_1, k_2…k_N are the rate constants for the corresponding transitions of kinetic intermediates, and k_A is the activation rate constant. (B) The activation time distribution with different numbers of kinetic intermediates. The time dependence of activation for $N > 0$ result in the inequality of activation rates in (C). (C) The rate of SOS activation as a function of the ratio between the mean dwell time and mean transition time. $k_A = 1\ s^{-1}$ in this numerical example. Short dwelling species has a lower activation rate than long dwelling species when $N > 0$, indicating that kinetic proofreading is in play.

3. Kinetic proofreading in membrane recruitment: single-molecule evidences

Activation of full length SOS (SOS^{FL}, interchangeable with SOS), a guanine nucleotide exchange factor (GEF), via Grb2-dependent recruitment is a prototypical example of a multidomain cytosolic protein that follows membrane recruitment-activation protocol[2] (20). SOS contains the general features of a multilayer regulations securing its autoinhibition in the cytosol, but can release its autoinhibition on membranes (12). The REM and CDC25 domains in SOS, enclosing both the allosteric and catalytic pocket for its substrate Ras, are flanked by C-terminus proline-rich (PR) domain and N-terminus Histone Fold (HF), Dbl-homology (DH) and Pleckstrin-homology (PH) domains gating SOS activity (Fig. 1a). The PR domain binds with the SH3 domains of Grb2 with a high affinity (K_d = 1 nM) (21), while the SH2 domain of Grb2 interacts with phosphotyrosine (pY) of membrane receptors such as LAT or EGFR (22). Upon membrane recruitment, interactions of N-terminus domains with anionic lipids such as PIP_2 and engagement of Ras at the allosteric pocket then release the autoinhibition (12), allowing processive catalysis of hundreds turnovers from a single recruitment event (23). While structural studies have led to insights about possible modes of activation, real-time dynamic studies of activation are missing for it requires an assay resolving the temporal process of recruitment and subsequent activation at the molecular level. Furthermore, the multilayer regulations of SOS necessitate full membrane reconstitution of SOS activation from phosphorylation of membrane receptors to downstream triggering (e.g. Raf recruitment) (5, 11, 12, 20) (Fig. 3-1A).

We developed a single-molecule activation assay to resolve the activation profile of SOS from membrane recruitment to initiation of Ras turnover (Fig. 3-1A). Lipids consisted of DOPC with 2% PIP_2, 2% MCC-DOPE and 4% Ni^{2+}-NTA-DOGS were deposited on a glass substrate. Cytoplasmic domains of Src kinase Hck and adaptor protein LAT with His_6 tag were tethered to Nickel-chelating lipids (24), while H-Ras were covalently attached to membranes via maleimide chemistry (25). Membrane proteins reconstituted on supported membranes were laterally fluid

[2] Contents in this chapter are in manuscript preparation (W.Y.C. Huang, S. Alveraz, Y.K. Lee, Y. Kondo, J.K. Chung, H.Y.M. Lam, J. Kuriyan, J.T. Groves).

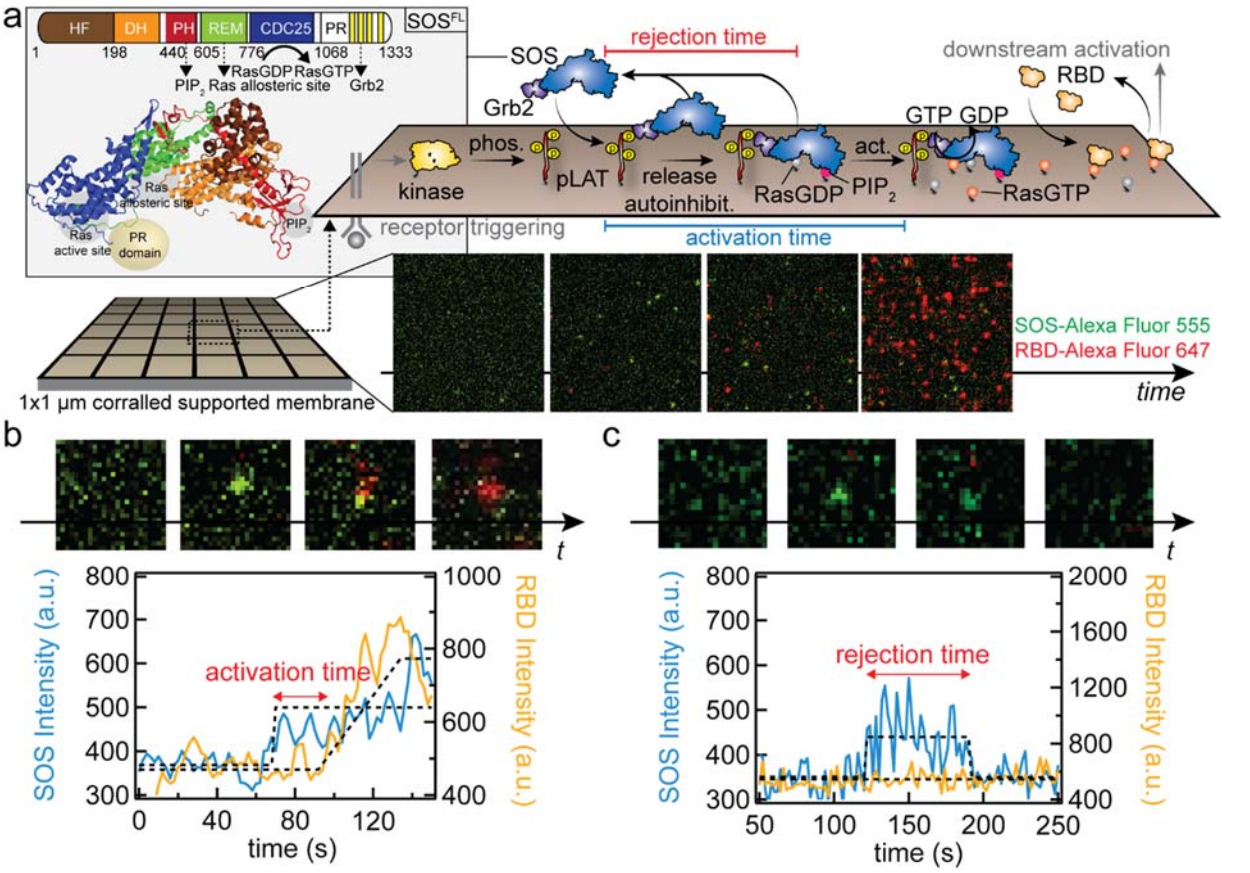

Fig. 3-1 Single-molecule activation assay of full length SOS on supported membrane. a, Schematic of the experimental setup. LAT phosphorylated by membrane-bound kinase Hck and Ras preloaded with GDP were decorated on the supported membranes corralled by 1 by 1 or 2 by 2 μm chromium grids. Injection of Grb2, SOS-Alexa Flour 555, RBD-Alexa Fluor 647 and GTP into the solution triggers SOS recruitment, release of autoinhibition and activation. SOS crystal structure rendered with PDB 3KSY. Images are snapshots of SOS (green) and RBD (red) recruitment during one experiment. **b,** Definition of activation time. **c,** Definition of rejection time.

with typical densities of <100, ~800, and ~500 μm^{-2} for Hck, LAT and Ras, respectively. Phosphorylation of LAT by Hck can be monitored with recruitment of fluorescent Grb2 (13). SOS^{FL} are prepared by indene ligation of N-terminus and C-terminus domains. By inclusion of 20 nM Grb2 and ~1 nM SOS in solution, single-molecule membrane recruitment of SOS via Grb2 can be clearly resolved on a total internal reflection (TIRF) microscopy. After a short period of time (tens of seconds), Ras preloaded with GDP were exchanged with GTP in solution, which enables dynamical binding of Ras-binding domain (RBD) derived from Raf-1 (40 nM in solution) onto membrane surfaces.

The reconstitution experiments can be performed on supported membranes corralled with 1 by 1 or 2 by 2 μm of chemically inert prefabricated chromium barriers (26). Lipids and membrane-anchored proteins were laterally fluid within a corral but restricted across different grids. Both LAT and Ras had little variations (< 15%) across different arrays. This microarray strategy allows

precise assignment of Ras turnovers to a single recruitment event of SOS (23), while retaining sufficient statistics to sample the activation profile.

Simultaneous imaging of SOS-Alexa Fluor 555 and RBD-Alexa Fluor 647 channels at the framerate of 0.5 Hz recorded the time sequence of when and where SOS recruitments and activations occured, from seconds to minutes (Fig. 3-1A). Specifically, we parse out corrals with SOS recruitment prior to RBD recruitment, and analyze their time sequence. The trajectories can be largely classified into two types: ***i)*** recruitment of SOS followed by activation indicated by RBD recruitments (Fig. 3-1B), and ***ii)*** recruitment and dissociation of SOS without activation (Fig. 3-1C). The first provides the activation time interval between membrane engagement and activation – which we defined as the activation time; the later indicates the membrane dwell times under the condition of no activation – which we defined as the rejection time. A single recruitment event must result in activation or rejection, yet the likelihood of either fate can be estimated probabilistically.

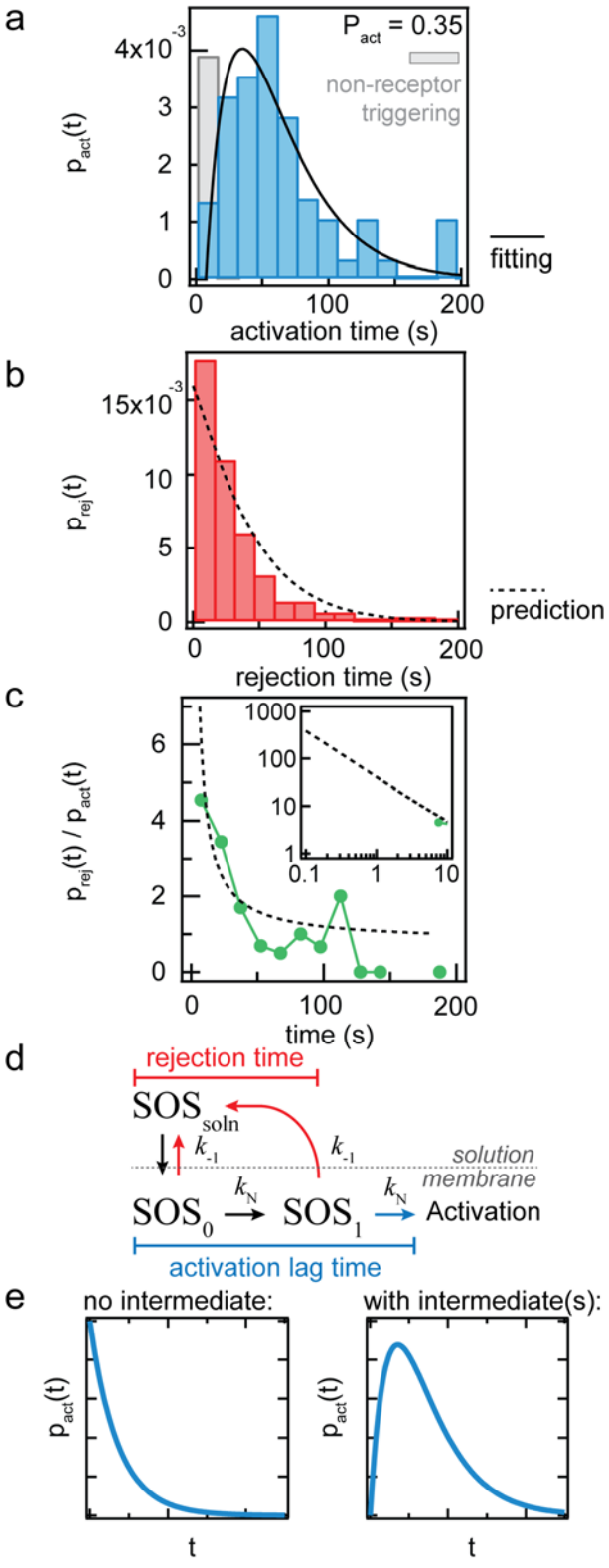

Fig. 3-2 Activation time distribution and kinetic proofreading in membrane recruitment. a, b, Histogram of activation time and rejection time of SOS activation via Grb2 recruitment from the single-molecule activation assay. **c,** The proofreading strength, denoted by the ratio between rejection and activation count, as a function of time. Solid line is fitting to the analytical model in **d**, the fitted values are k_N = 0.02 s^{-1} and k_{-1} = 0.016 s^{-1}. Dash lines are prediction by the model without fitting. **d,** Activation of SOS on membranes is a competition between activation kinetics and dissociation from the membranes. k_N denotes the transition rate constants for the kinetic intermediates and k_{-1} is the dissociation rate constants from membranes. **e,** Without an kinetic intermediate (N = 0), activation time distribution resembles an exponential-like distribution peaked at t = 0. Having at least one intermediate gives a characteristic rise-and-decay gamma-like distribution for activation time distribution.

The underlying mechanism of SOS activation can be inferred by measuring the distributions and statistics of the activation profiles. By collecting hundreds of these trajectories, we compiled the histograms of the activation and rejection distribution (Fig. 3-2AB). The activation time distribution shows a rise-and-decay Gamma-like distribution with a mean of 55 ± 44 sec (± denotes standard deviation) (Fig. 3-2A). The resolution of detectable activation time in this assay is on the order of a few seconds, inferred from: ***i)*** the fast binding kinetics (~100 ms) of RBD and, ***ii)*** non-receptor triggering (discussed in details later) shows trajectories of simultaneous SOS recruitment and RBD binding without detectable interval from 0.5 Hz framerate. The rejection time distribution exhibits an exponential-like distribution with a mean of 30 ± 29 sec (Fig. 3-2B). The distributions are further analyzed by considering an analytical model of SOS activation.

The main features of membrane-dependent activation of SOS, or any other autoinhibited cytosolic enzyme, can be described by the competing kinetics between activation pathway and dissociation from membrane surfaces (Fig. 3-2D) (Chapter 2) (13, 16, 17). Given *N* number of kinetic intermediate(s), the activation time distribution is

$$p_{act}(t) = p_N(t) \cdot e^{-k_{-1}t} \quad [3.1]$$

where $p_N(t)$ is the activation time for a multistep process from convolution of *N* single Poisson steps, and k_{-1} is the dissociation rate constant. To gain an intuition about the shape of the distribution, we consider the limiting case where the transition rate constants (k_N) of each step is identical, leading to analytically extractable $p_N(t) = k_N^{N+1} t^N e^{-k_N t}/N!$, a Gamma distribution of rise-and-decay feature (Fig. 3-2D). However, in the opposing case without any kinetic intermediates ($N = 0$), the activation time distribution is strictly exponential (Fig. 3-2D). The observed data is consistent with the first case, indicating that activation of SOS on membranes involves progressing through kinetic intermediate with a slow transition rate (k_N) of about 0.02 s^{-1}. In practice, the kinetic observation will be dominated by the slowest kinetic progression step. Thus, we use $N = 1$ to analyze the distributions, i.e. $p_{act}(t) = k_N^2 t e^{-(k_N + k_{-1})t}$. To validate the model, we use it to predict the rejection distribution prior to the knowledge of the data. The rejection time distribution can be shown to be

$$p_{rej}(t) = \frac{\Gamma(N,t)}{N!} \cdot k_{-1} e^{-k_{-1}t} \quad [3.2]$$

where $\Gamma(N,t) = \int_{k_N t}^{\infty} t'^N e^{-t'} dt'$, the upper incomplete Gamma function. In the case of $N = 1$, $p_{rej}(t) = k_{-1}(k_N t + 1)e^{-(k_N + k_{-1})t}$. Strikingly, the general features of the rejection distribution is well described by the prediction (Fig. 3-2B), suggesting that activation and dissociation kinetics are the main competing processes in SOS activation. It is worth reminding ourselves that this model does not exhaust all possible routes or details of activation but only delineate the main pathway.

Next, we evaluate the signaling consequence of the observed activation profile, specifically by verifying the inclusion of kinetic intermediates can result in kinetic proofreading. Modeling shows that the ratio of $p_{rej}(t)/p_{act}(t)$, which we termed as the proofreading strength, is a monotonically

decaying function of time (for $N = 1$: $p_{rej}(t)/p_{act}(t) = k_{-1}(k_N t + 1)/(k_N^2 t)$), indicating the capability of exhibiting kinetic proofreading, i.e. events dwelling longer has a higher probability to activate. This trend is also embedded in the experimental observation (Fig. 3-2E). Together, the data and model provide a self-consistent statement of how a multistep process can exhibits kinetic proofreading. The general kinetic topology is similar to the classical kinetic proofreading proposed by Hopfield (14) but differs slightly in the implementation of conditions: there is no ATP-consumption in the actual proofreading steps (yet preparation of one-way trafficking of SOS (20) may require energy for an actual living system).

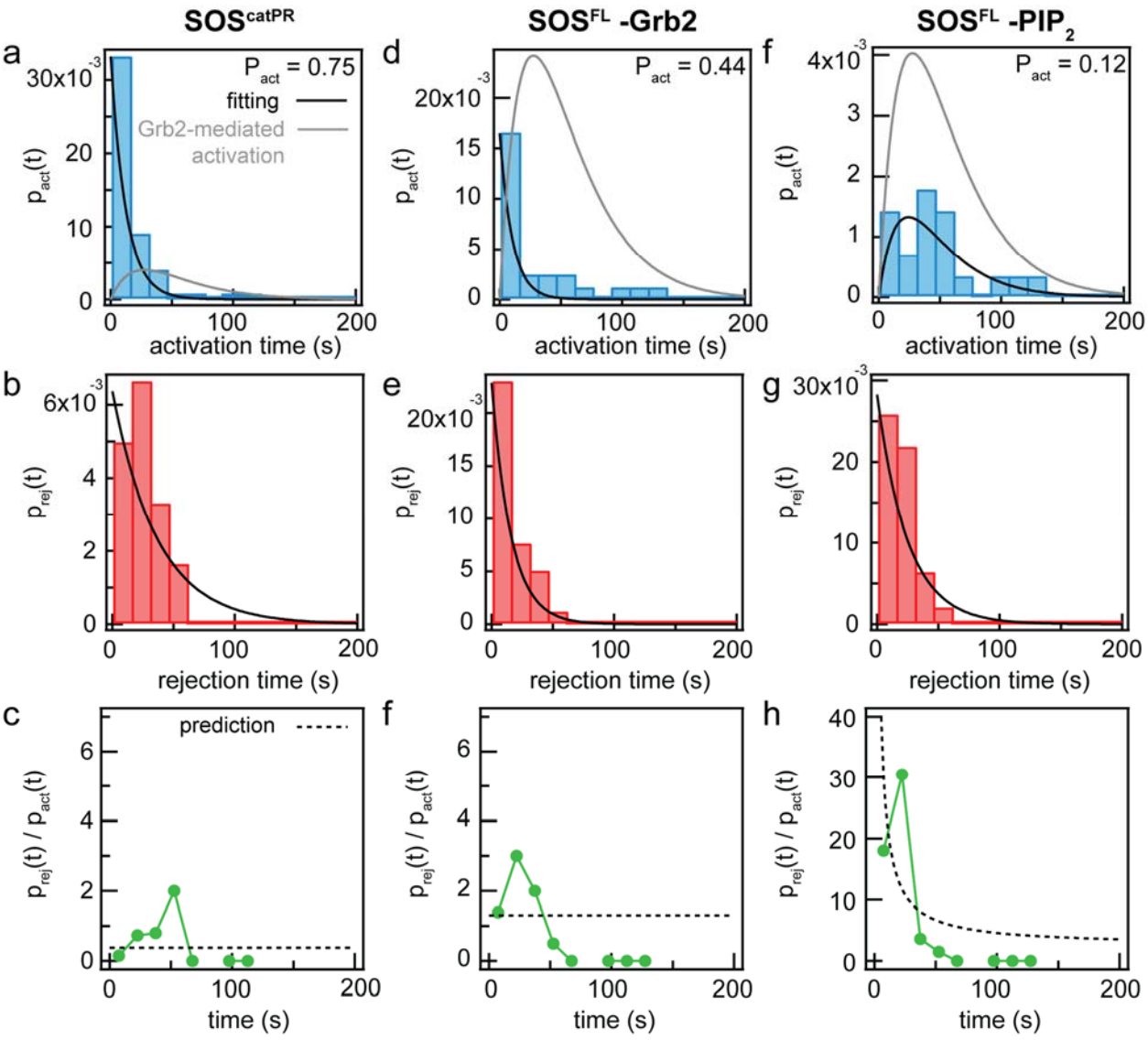

Fig. 3-3 Activation process is mediated by the autoinhibition state of SOS. The activation distribution (**a**, **d**, **f**), rejection distribution (**b, e, g**), and proofreading strength (**c, f, h**) for SOS activation without PIP2 (**a-c**), without Grb2 (**d-f**) and SOScatPR (**f- h**). Grb2-mediated activation for **d** is scaled by consideration of the concentration effect from non-receptor activation.

The activation pattern can be modulated by different modes of recruitment, regulated by the autoinhibition state of SOS. The initial engagement state (SOS_0) is mediated primarily by Grb2, while the slowest kinetic bottleneck (SOS_1) involves release of autoinhibition by PIP_2-mediated structural rearrangement (Fig. 3-4A), inferred from the following observations: ***i)*** Grb2 independent activation is a single step activation process (its activation time distribution is exponential) bypassing SOS_0 (Fig. 3-3, 3-4), ***ii)*** SOS^{catPR}, lacking full autoinhibition, leads to increased activation of first-order kinetics by bypassing the necessity to release autoinhibition (SOS_1) (Fig. 3-3, 3-4) and, ***iii)*** absence of PIP_2 significantly decreases the activation rate yet retaining the kinetic bottleneck (Fig. 3-3, 3-4). In each cases, the proofreading strength also follows the qualitative prediction of the model: case ***(i)***, ***(ii)*** and ***(iii)*** corresponds to decrease, decrease and increase in proofreading strength, respectively. Assignment of molecular states to SOS regulation provides a useful framework (Fig. 3-4) for future evaluation of how SOS mutants or drugs modulate the functionality of SOS.

Assays of this type show that membrane recruitment of autoinhibited proteins requires some finite time to activate, which naturally implement kinetic proofreading in the recruitment process. One important consequence is that membrane dwell times, or more broadly recruitments, are disproportionate to activation itself.

Kinetic proofreading in recruitment process raises the question of how cellular network can actively distinguish between genuine receptor signals and molecular noise. Recent single-molecule dwell time studies have shown that molecular assembly, driven by multivalent phosphotyrosine LAT interactions, drastically enhances the dwell times of Grb2 and SOS by orders of magnitude (13). This kinetic enhancement is estimated to increase the rate of SOS activation by 10-50 fold under the gatekeeping of kinetic proofreading. This type of regulation provides means to detect robust activation in a noisy environment based on dynamical discrimination.

The concepts and methods developed in this work should be applicable to a wide range of cytosolic enzyme in signal transduction, for example N-WASP (27) in actin regulation or ITK (28) in Ca^{2+} flux triggering. More broadly, first-passage analysis of this kind resolving the temporal discrimination process can be applied to evaluate the role of enzymology in signal transduction.

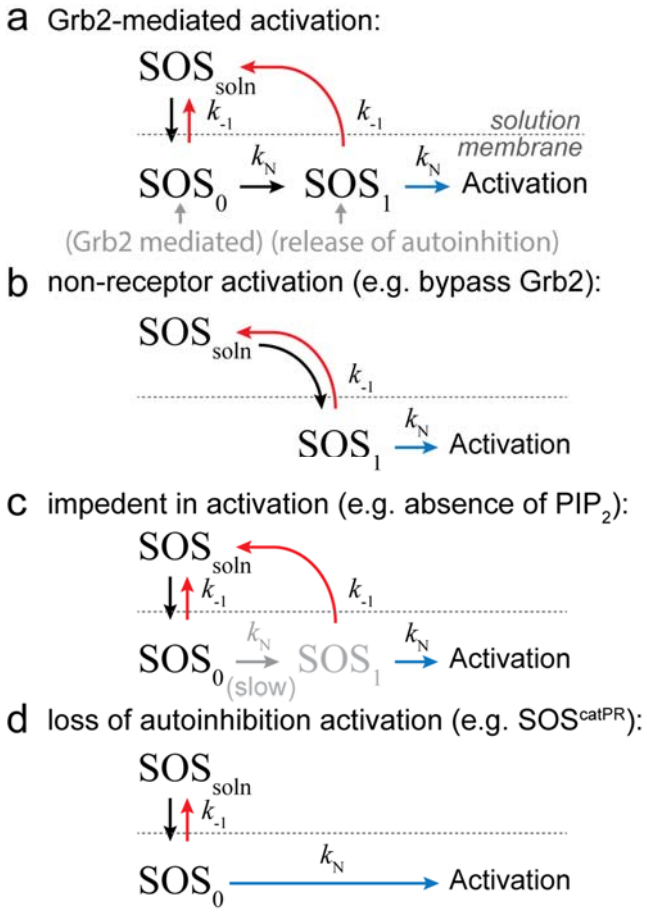

Figure 4 | Modulation of activation pathway

4. Molecular assembly: a mechanism to tune kinetic proofreading

Assembly of receptors with adaptor proteins and effectors has been well documented in multiple signal transduction systems. Some examples include the growth factor receptors (2, 29), components pertaining to actin cytoskeleton reorganization (30), Ephrin receptors (10, 31-35), and membrane receptors in T cells (3, 36, 37). In each of these systems, the signaling molecules contain repetitive multivalent protein-protein interaction domains that drive the extended assembly of molecular complexes during signal transduction. Tyrosine phosphorylation is a prototypical mediator of such assembly.

In the case of T-cell receptor (TCR) signaling, linker for the activation of T cells (LAT) has several tyrosines (Y) that are phosphorylated upon TCR triggering. Three of these (Y171, Y191 and Y226) are known to recruit the cytosolic adaptor protein, growth factor receptor-bound protein 2 (Grb2), by its SH2 domain (22). Grb2 additionally has two SH3 domains, which bind to the proline-rich regions in the C-terminal domain of the nucleotide exchange factor, Son of Sevenless (SOS) (38). A single SOS molecule can associate with at least two Grb2 molecules (1), enabling the LAT:Grb2:SOS interactions to form an extended network assembly on membranes upon LAT phosphorylation (1, 39-41) (Fig. 4-1). Similar assemblies have been reconstituted *in vitro* for the nephrin:Nck:N-WASP system on two dimensional membrane surfaces (30, 42). In live cells, introduction of mutations that reduce the multivalency in the LAT:Grb2:SOS assembly alter the spatial pattern of the receptors (1, 43) and disrupt the downstream signaling (44, 45). Although the existence of these signaling assemblies is documented, the physical mechanisms by which they modulate signal transduction remain unclear.

4.1 Kinetic bifurcation from molecular assembly[3]

Since assembly intrinsically involves increasing the local concentration of molecules, it is often thought that this will lead to enhanced reaction kinetics and therefore facilitate signal propagation. However, this conclusion is based on the assumption that dynamical parameters of the system, such as molecular binding kinetics and diffusive mobility, are unchanged in the condensed

[3] Contents in this section are published in Huang *et al. PNAS*, 2016, **113**:8218.

structure. In fact, we would expect such dynamical parameters to be strongly modulated by assembly—thus offering various possibilities for the ways assembly may enhance, inhibit, or conceivably redirect signaling. Actual quantitative measurements of such kinetic properties are sparse (6, 43, 46). Here we reconstitute phosphotyrosine-mediated LAT:Grb2:SOS assembly on supported membranes with the purpose of performing a quantitative analysis of how the extended network assembly influences the molecular kinetics of Grb2 and SOS recruitment.

Measurements of single-molecule binding dwell time distributions reveal two, well-differentiated, kinetic species for both Grb2 and SOS on LAT assemblies. The majority fraction of membrane-recruited Grb2 and SOS both exhibit fast single exponential kinetics, with average dwell times of hundreds of milliseconds. These kinetics are nearly identical with those observed in the unassembled state, and thus correspond to monovalent binding interactions. A subpopulation of the molecules, however, exhibits much slower binding kinetics, with dwell times extending to tens of seconds. These long-lived Grb2 and SOS binding events arise from multivalent interactions within the LAT:Grb2:SOS assembly.

Activation of the Ras GEF activity of full length SOS involves a multistep process (12). Following membrane recruitment by Grb2, structural rearrangements within SOS expose lipid binding domains that stabilize the protein on the membrane, expose the allosteric Ras binding site, and release autoinhibition of SOS guanine nucleotide exchange activity. Once fully activated, SOS remains on the membrane and processively catalyzes nucleotide exchange on many Ras molecules (23). Since SOS activation requires a sequence of events, its activation is subject to a type of kinetic proofreading (14, 47), by which molecules that dwell on the membrane for longer periods of time are disproportionately more likely to become activated. A corollary of this fact is that for the same total amount of membrane recruited SOS, more SOS molecules will become activated if a slow kinetic species exists—or in the extreme case, only the slow kinetic species activate. The slow kinetic species of membrane recruited SOS, which is here uniquely observed in phosphotyrosine-mediated LAT assemblies, could thus correspond to the activating condition for this molecule. This would have the effect of limiting SOS activation to regions of genuine receptor triggering and the resultant LAT assembly, while reducing the probability of

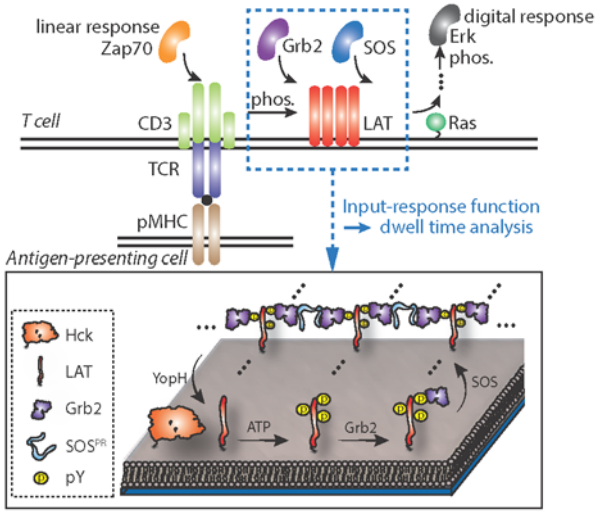

Fig. 4-1 Quantification of the input-response function of LAT:Grb2:SOS assembly in TCR signaling. Schematic of TCR signaling pathway (top) and the in vitro reconstituted system (bottom). Engagement of TCR with pMHC results in phosphorylation of LAT, which triggers assembly reaction on the cytoplasmic side of the plasma membrane. LAT assembly promotes SOS membrane recruitment and activation, which propagates downstream signals. To quantitatively assess the input-response function at the LAT signaling node, the signaling geometry of LAT is reconstituted on supported membranes. Phosphorylation of LAT is triggered by membrane-bound tyrosine kinase Hck, which results in Grb2 recruitment. The assembly reaction is initiated by the addition of SOS proline-rich domain and can be reversed by tyrosine phosphatase, YopH.

spontaneous SOS activation elsewhere on the cell membrane. The generality of this type of kinetic proof reading suggests that such a mechanism may be at play in multiple receptor proximal signaling processes.

Phosphotyrosine-mediated LAT:Grb2:SOS assembly on supported membranes

In the following experiments, the cytoplasmic domain (residues 30 to 233) of LAT is purified with an N-terminal 6-His tag and chemically modified with a maleimide fluorophore (Alexa Fluor 555) at Cysteine 146 (with a labeling efficiency of 60%). This His6-LAT, here referred to as LAT, can be stably linked to supported membranes containing Ni-NTA lipids (4 mol %) (24). The membrane associated LAT is laterally diffusive, as characterized by fluorescence recovery after photobleaching (FRAP) experiments and single-molecule tracking (SMT). A single diffusive population with diffusion coefficients of ~1.8 $\mu m^2/s$ is typically observed, indicating that LAT behaves as a monomeric molecule on supported membranes (25). Surface densities of LAT can be controlled from 100-5000 molecule/μm^2 and were calibrated by fluorescence correlation spectroscopy (FCS). In these experiments, LAT is phosphorylated by membrane-tethered Src family kinase Hck. The phosphorylation reaction is monitored by the membrane recruitment of full length Grb2 coupled to a fluorophore (Alexa Flour 647) using maleimide-thiol chemistry at Cysteine 32 (with a labeling efficiency of 95%). On a total internal reflection fluorescence (TIRF) microscope, Grb2 recruitment reports the phosphorylation of LAT in real time; LAT:Grb2 exhibits relatively fast binding kinetics (k_{-1} = 1.5 s^{-1}) compared to the phosphorylation reaction (~ 1-2 min). Other kinases, including Zap70 (48), can also be used to phosphorylate LAT without appreciable differences detectable by Grb2 binding.

A macroscopic network assembly of phosphorylated LAT (pLAT) forms on the membranes when the proline-rich domain (residues 1051 to 1333) of SOS (abbreviated as SOS) and Grb2 are both present in the solution (Fig. 4-1, 4-2A). Assembly depends on the solution concentrations of Grb2, SOS and the membrane surface density of pLAT. Using 5.8 μM Grb2 and 1.45 μM SOS (the ratio of the concentrations for Grb2 and SOS is fixed to 4 for all experiments) over a pLAT density of about 2400 molecule/μm^2, small mobile puncta of highly dense LAT emerged

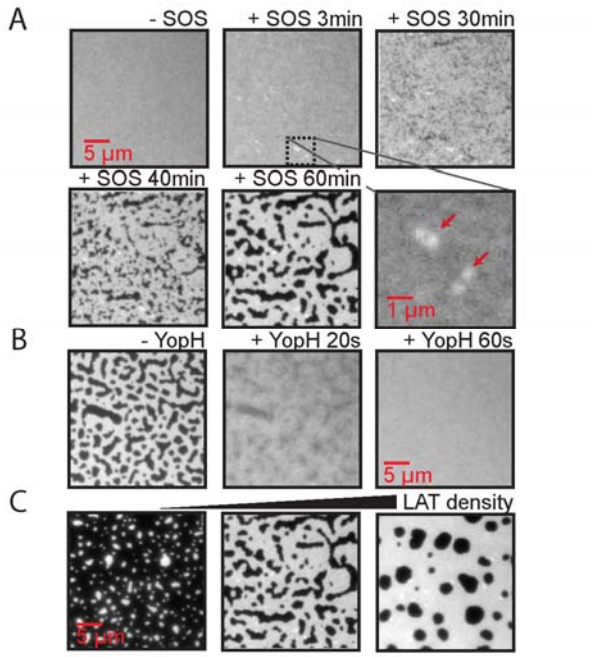

Fig. 4-2 LAT:Grb2:SOS is sufficient to drive an assembly network on membrane surfaces. (A) Epifluorescence images of LAT undergoing an assembly reaction. After injection of 5.8 μM Grb2 and 1.45 μM SOS, small puncta of densely assembled proteins (red arrow) appears within a few minutes. The emergence of a macroscopic protein-dense phase was observed after 30 minutes. (B) Reversibility of the assembly. The phase boundary disintegrated abruptly into a homogenous phase after incubation of 10 μM phosphatase YopH. (C) Different geometries and sizes of LAT assemblies by manipulating the surface densities of LAT ranging from 600-4000 molecule/μm^2 in the presence of 5.8 μM Grb2 and 1.45 μM SOS.

across the membrane within 3 minutes of mixing (red arrow in Fig. 4-2A). These subsequently evolve into a macroscopic protein-dense phase (with an estimated density of ~4000 molecule/μm^2) that is interspersed with regions void of LAT (Fig. 4-2A). The assembly is dynamic; FRAP measurements on LAT reveal recovery of intensity in photobleached spots (diameter 21 μm, τ_D = 704 s, $D_{effective}$ = 0.20 $\mu m^2/s$). The assembly is governed by multiple tyrosine phosphorylation of LAT, as confirmed by the following observations: ***i***) Kinase dependent LAT phosphorylation is required for assembly formation, ***ii***) LAT mutants containing only a single Grb2 accessible phosphotyrosine site fail to form the assembly under the same experimental conditions, ***iii***) Introduction of a tyrosine phosphatase (10 μM YopH) in the solution rapidly reverses this entire process, within a minute (Fig. 4-2B), eliminating Grb2 recruitment to LAT and driving the system back to a uniform and fluid distribution of LAT on the membrane. FRAP experiments on LAT prior to assembly and after dephosphorylation reveal similar free mobilities, with τ_D values of 113 s (D = 1.26 $\mu m^2/s$) and of 115 s (D = 1.24 $\mu m^2/s$), respectively.

This type of phosphotyrosine-mediated condensation and assembly resembles a gelation phase transition (30, 42). Theoretical studies of the LAT:Grb2:SOS system specifically predict the existence of a gelation phase transition (39). Leaving the details of whether or not the condensed phase experimentally observed here meets the technical definition of a gel phase (49) to a later discussion, the transition itself is empirically discrete. We experimentally map its effective phase diagram as a function of LAT, Grb2, and SOS concentrations. The assemblies can form with a LAT density as low as ~600 molecule/μm^2. Macroscopic features of the condensed phase, such as the domain size, geometric distribution, and fractional area coverage can be controlled by the average LAT density (Fig. 4-2C). However, intensive properties such as molecular binding kinetics should be independent of the size of LAT assembly. With single-molecule dwell time measurements on different sizes of LAT assemblies, we affirm that the binding kinetics of these assemblies are not influenced by their macroscopic geometry. The LAT assembly exhibits essentially the same molecular level behavior regardless of its large-scale shape and appearance. We therefore take advantage of the extended assembled structures (a few microns in size) for better spatial resolution for single-molecule measurements, described below.

Kinetic bifurcation of Grb2 and SOS membrane dwell time from single-molecule analysis

TIRF imaging of fluorescently labeled (Alexa Fluor 647) Grb2 or SOS enables observation of membrane recruitment, movement on the membrane surface, and desorption, at the single molecule level (Fig. 4-3B). Single-step photobleaching, determined unambiguously with a Bayesian algorithm (50), verified that the tracked objects were single molecules (Fig. 4-3B). In the case of simple bimolecular kinetics of pLAT:Grb2, a single population of short, exponentially distributed, dwell time is observed. The mean dwell time, 0.65 s (acquired at a framerate of 21 Hz), corresponds to an ensemble kinetic off rate ($k_{-1,pLAT:Grb2}$) of 1.5 s^{-1}, after correction for the measured photobleaching rate (Fig. 4-3C).

For analyses of Grb2 and SOS kinetics on the LAT:Grb2:SOS assembly, we acquire Grb2 or SOS single-molecule images during the quasi-stationary state, in which the assembly exhibits a stable geometry with only local phase boundary fluctuations (Fig. 4-4). The assembly produces a notable

affect on the recruitment rate of Grb2. At a fixed Grb2 solution concentration of 5.8 μM and a pLAT membrane density of ~2400 molecule/μm^2, the presence of SOS (1.45 μM in solution) leads to a 5-fold faster rate of Grb2 recruitment. We also observe an enhancement in the membrane-bound Grb2:SOS ratio, which is >10:1 in the assembly compared with the bulk concentration ratio of 4:1. These observations were made using two-color imaging of Alexa Fluor 647 labeled Grb2 and Atto 488 labeled SOS, The enhanced recruitment could be attributed to the increased affinity of SOS-bound Grb2 to pLAT (51), the presence of membrane-bound SOS (providing more binding sites), or physical alterations in the structure and accessibility of pLAT in the assembly.

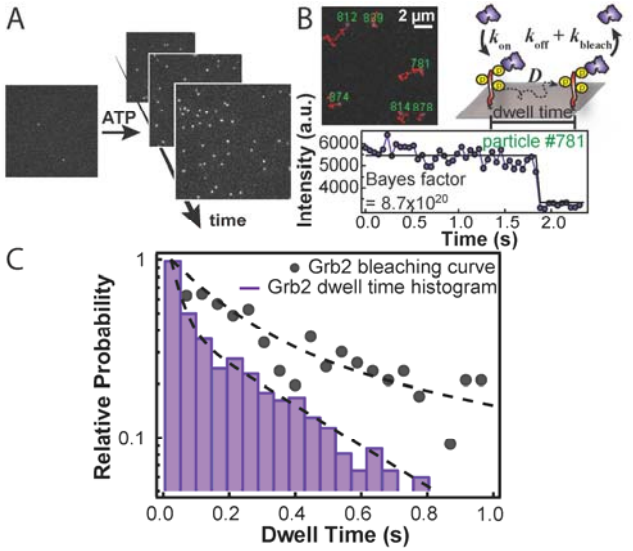

Fig. 4-3 Input-response function parameterized by single-molecule dwell time analysis. (A) Single-molecule images showing the gradual increase in Grb2 recruitment following LAT phosphorylation. (B) Diffusion and dissociation kinetics for membrane recruited Grb2 measured from single-particle tracking. Single-step photobleaching confirmed that the tracked Grb2 is a single molecule. The existence of a change point was detected using a Bayesian algorithm. (C) Dwell time histogram of Grb2 (purple histogram). After correction of photobleaching (black dots), the dwell time of LAT:Grb2 is 0.65 ± 0.10 s, setting the baseline of the input-response function prior to any assembly structure. Dash line is fitting to a single kinetic population.

The dwell time distributions for both Grb2 and SOS are altered on the LAT assemblies. Specifically, a second kinetic species with dwell times two orders of magnitude longer for both proteins emerges (Fig. 4-4A). At a framerate of 2 Hz, the slow kinetic species is resolved clearly. Apparent dwell times of the long-lived Grb2 ranged from 10-100 s. Mapping trajectories of molecules with dwell times greater than 10 s reveals highly constrained motion within the network assembly (Fig. 4-4C). Furthermore, the dwell time distribution deviates from a single exponential (Fig. 4-4A), which implies that the long dwelling species is a convolution of multiple binding states. For both Grb2 and SOS, the long-lived species represents only a minor fraction (population fraction < 0.1) of the total amount of membrane recruited protein; the majority fraction still exhibits fast kinetics. At a framerate of 21 Hz, the fast kinetic species is clearly resolved and proves to be identical to that of the monovalent binding kinetics of pLAT:Grb2 described above (Fig. 4-4A).

The long-lived SOS species exhibits longer dwell times than those observed for Grb2 ($\langle\tau_{SOS}\rangle$~29.3 s, $\langle\tau_{Grb2}\rangle$~10.8 s, estimated from trajectories with an apparent dwell time greater than 3 s) (Fig. 4-4A). This mismatch in dwell time indicates that Grb2 and SOS are not in a stable complex on the membrane over the timescale of seconds. Instead, the molecules must undergo dissociation and rebinding processes in the assembly such that the long dwelling SOS species interacts with multiple membrane-bound Grb2. Incidentally, the timescale of the long-lived SOS is comparable to the slow transition rate between different active SOS conformations observed in single-molecule studies of SOS activation of Ras (23, 52). The majority fraction of recruited SOS

also exhibits fast kinetics (Fig. 4A), although comparison to the monovalent binding kinetics of Grb2:SOS is unlike the simple case of pLAT:Grb2. Nonetheless, by assuming that the fast kinetic species corresponds to the monovalent interaction, we estimate $k_{\text{-1,Grb2:SOS}} = 0.47\ s^{-1}$ from $k_{\text{app,SOS}} = k_{\text{-1,Grb2:LAT}} + k_{\text{-1,Grb2:SOS}} + k_{\text{bl,SOS}}$, where $k_{\text{app,SOS}}$ is the apparent dissociation rate and $k_{\text{bl,SOS}}$ is the photobleaching rate.

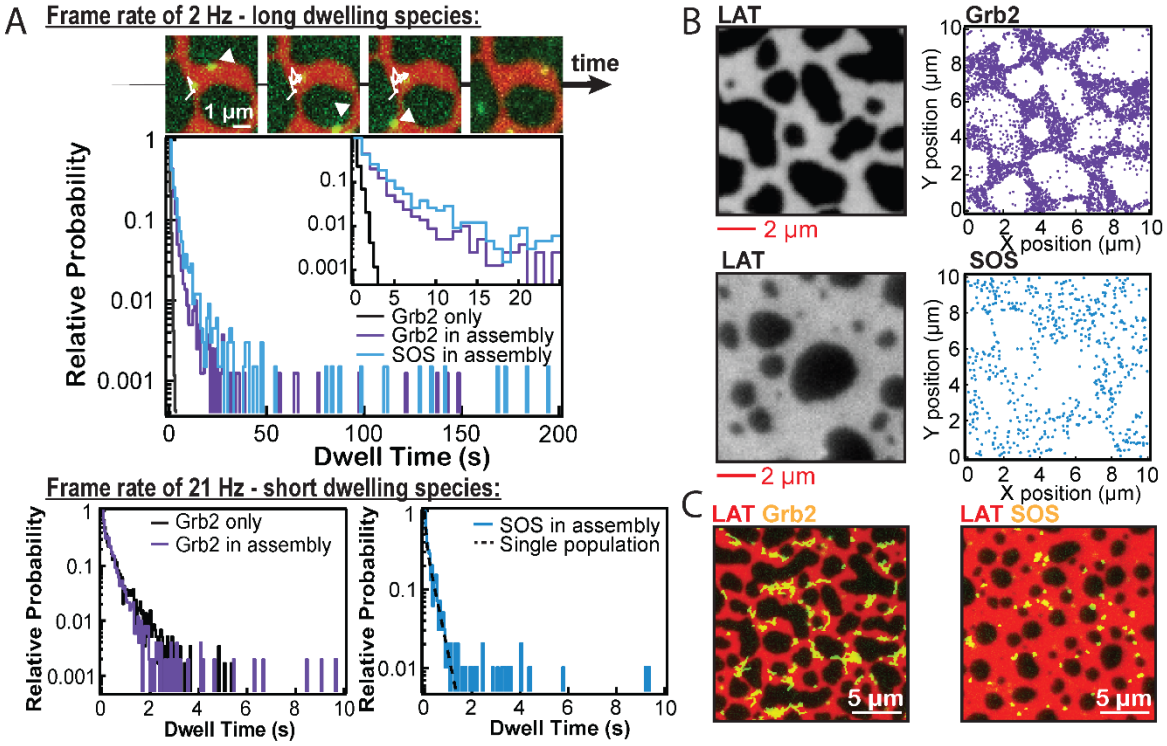

Fig. 4-4 Protein assembly creates kinetic bifurcation in the recruitment dynamics of Grb2 and SOS. (A) The kinetic species of interest are evaluated at the two different frame rates of 2Hz and 21Hz. The top lane shows the time-lapse imaging of Grb2 and SOS at the framerate of 2 Hz. The assembly structure is marked by labeled LAT (red). Membrane-bound Grb2 (yellow) exhibits two kinetic populations: (1) short dwell times (white arrow), and (2) long dwell times (white tracks). The statistics are summarized in the dwell time histograms: (1) Grb2 prior to assembly structure (black) and, (2) Grb2 in protein assembly (purple) and, (3) SOS in protein assembly (blue). The bottom row shows dwell time histogram of Grb2 and SOS in protein assembly acquired at the framerate of 21 Hz. The fast kinetic species of Grb2 in protein assembly (purple) exhibits identical rate as the binding kinetics of pLAT:Grb2 prior to assembly (black). The fast kinetic species of SOS (blue) is also well described by a single kinetic population, with a fitted $k_{\text{app,SOS}}$ of 3.4 s^{-1}. (B) Grb2 and SOS are recruited to the LAT assembly. Strong correlations are observed between epifluorescence images of LAT (left) and the reconstructed images of Grb2 (right top) and SOS (right middle), obtained by compiling all single-molecule recruitment events within 400 s. (C) By mapping trajectories with apparent dwell time greater than 10 s onto the LAT patterns (bottom), it is evident that the long dwelling species localize to the assembly structure.

Discussion

Single-molecule dwell time analysis reveals two, well differentiated, kinetic species of Grb2 and SOS in the LAT:Grb2:SOS assembly. The fast kinetic species corresponds to the monovalent

interaction while the long dwelling species stems from multivalent engagement within the networked assembly. Motivated by these observations, we then ask if the elongation of dwell times can have a qualitatively different functional consequence, specifically in terms of the activation probability of the recruited effectors. More broadly, can kinetic stabilization from protein assembly be utilized by biochemical networks to distinguish genuine receptor-triggered signals from molecular stochastic noise? If so, what are the mechanistic requirements? We evaluate these questions analytically in the following by considering the activation process of SOS on the membrane surfaces.

Control of SOS activity on membranes is multilayered (11, 12). After Grb2-dependent membrane recruitment, SOS activation requires the release of autoinhibition, which involves conformational changes to expose lipid binding domains and the engagement of Ras at the allosteric binding pocket of SOS. This multistep process all but guarantees the existence of one or more kinetics intermediates. It is thus natural to presume that a finite amount of time is required for SOS to be fully activated following initial membrane recruitment. Following analysis in Chapter 2, single-molecule and structural studies of SOS provide an estimation of the physical parameters in the model. Considering the case where the activation pathway of SOS involves two kinetic intermediates (release of autoinibition by the N-terminal domains and engagement of Ras in the allosteric binding site) (25, 35) with slow transition rates ($N = 2$, $k_N = 0.1$ s^{-1}) (26, 34), we estimate a 60-480 enhancement factor in the activation rate when the dwell time is elongated from 0.1 s to 1-100 s for the same total amount of membrane recruited SOS. Although the exact value of the parameters in cells are not known, this model allows us to estimate the potential strength of kinetic proofreading from a range of plausible parameter values. From the analysis, elongation of membrane dwell times of SOS in association with LAT assembly therefore implicates LAT assembly as a possible gatekeeping mechanism that limits Ras activation through kinetic proofreading in the activation of SOS (Fig. 4-5). The need for such restriction in SOS activation is underscored by recent single molecule SOS:Ras activation studies, which demonstrate that a single SOS molecule is capable of processively activate thousands of Ras in a single membrane recruitment event (23).

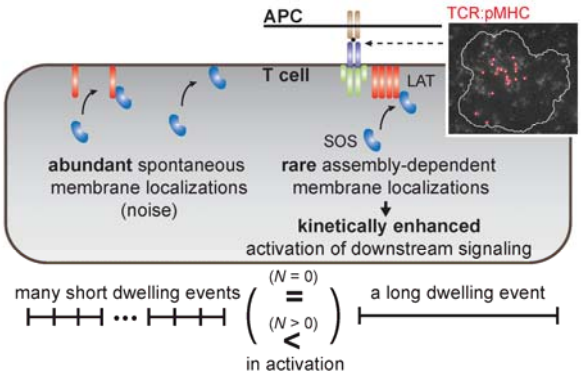

Fig. 4-5 Assembly-dependent membrane recruitments can achieve kinetic proofreading. Assembly-dependent modulation of membrane dwell times can control the activation rate of cytosolic enzyme such as SOS. Kinetic proofreading of SOS ensures that receptor-dependent triggering events are distinguishable from spontaneous membrane localizations. This accuracy is especially important in TCR triggering, where detection of low agonist densities is crucial (the top right image shows that low density of TCR:pMHC complex can lead to activation). Regulation of the recruitment dynamics of biochemical networks through protein assembly thus provides a mechanism for controlling the amplification and noise filtration in signal transduction.

This statistical concept of kinetic proofreading here resembles to that first proposed by Hopfield (14). A classic example of its basic implementation is found in the triggering requirement for voltage-gated ion channels (53). In the context of TCR signaling, kinetic proofreading based on multiple

phosphorylation events on the TCR ITAMs in response to ligand engagement has been proposed to play a role in antigen discrimination based on peptide MHC:TCR binding kinetics (19). Although the kinetic topology of SOS activation model is similar to Hopfield's, it differs slightly in two aspects: ***i***) no energy consumption is necessary, yet a directionality of enzyme trafficking is required (a non-equilibrium process), ***ii***) proofreading is achieved by competition between the overall activation kinetics and dissociation (Eq. 1), instead of the kinetics of each intermediate complex.

Signal propagation in the TCR system exhibits an analog-to-digital conversion (8). Positive feedback from allosteric activation of SOS has been identified as a key element of this digitization (54). Here we show that, prior to the GEF activity of SOS, LAT assembly leads to kinetic bifurcation in the recruitment dynamics of SOS, in which the activation kinetics inherently exhibit qualities necessary to enable kinetic proofreading. In addition, extension of dwell times also suggest that bifurcation in the dynamics may be a fundamental mechanism that can promote the digitization of signal transduction. Taking a broader perspective, these basic characteristics of signaling assembly and multistep activation are not unique to the TCR system. They can be found in many other systems as well including, for example EGFR:Grb2:SOS (29) and nephrin:Nck:N-WASP (30).

After establishing the kinetic consequence of molecular assembly, we now revisit the identity of these assembly structure.

4.2 Molecular assembly has a dynamical structure of an entangled polymer[4]

Extensive networks of weak and rapidly reversible (e.g. ~500 ms for SH2:pY) interactions have manifested in both 2- and 3-dimensional apparent phase transitions in reconstituted systems (13, 30, 42, 55). The static connectivity of molecular assembly is analogous to a polymer, and assembly formation has been hypothesized to be a gelation phase transition (39) (a transition in connectivity in which a polymer can proliferate into an infinite network (49, 56)). Alternatively, the rapid turnover of individual molecules within the assembly, along with the visible macroscopic physical property of surface or line tension, has led to their description as viscous fluids (42, 57). These different possibilities have distinct dynamical properties with correspondingly different potential effects on chemical kinetics of signaling reactions. Detailed examination of the dynamic scaling of molecular mobility offers one approach to determine the molecular-scale structural identity of the assembly. In particular, the dynamical scaling law, defined as k in $\langle r^2 \rangle \propto t^k$ where r is distance traveled by an individual molecule (49), is an experimentally measurable property relating to both molecular structure as well as the diffusion process within the biochemical reaction itself.

In this section, the translational motion of individual LAT proteins engaged in the LAT:Grb2:SOS networked molecular assembly on supported membranes is comprehensively studied by single molecule tracking (SMT). LAT is a scaffold protein in the T cell receptor signaling system with nine tyrosine residues, three of which are known to recruit Grb2 after phosphorylation. Activation of T cell receptors by ligand leads to activation of the Zap70 kinase, which phosphorylates LAT. This occurs against a background of LAT dephosphorylation by phosphatase activity with the

[4] Contents in this section are in manuscript preparation (W.Y.C. Huang, H.-K. Chiang, N. Shah, J. Kuriyan, J.T. Groves

overall degree of LAT phosphorylation thus dynamically regulated by this kinase-phosphatase balance. This balance ultimately tunes the threshold for propagating a signal from the T cell receptor to downstream components of the signaling pathway. Grb2 contains SH2 and SH3 domains, enabling it to simultaneously bind pY residues on LAT and proline rich regions on SOS. SOS can bind to at least two Grb2 molecules, enabling extended network assembly as long as the LAT proteins are sufficiently phosphorylated (Fig. 4-6).

Phosphorylated LAT proteins reconstituted on supported membranes are laterally fluid and coalesce into assembled structures upon addition of Grb2 and SOS. This phase transition is reversible by addition of phosphatase and the structure is dynamically controlled by the degree of LAT phosphorylation (13, 55). We measure the dynamical scaling law of LAT movement on membranes and observe subdiffusive motion ($\langle r^2 \rangle \propto t^k$ where $k < 1$) of LAT in the assembly only below a characteristic timescale. Multiple subdiffusive timescales can be resolved with faster image acquisition rates. Comparing these results with Monte Carlo simulations and classical polymer theory reveals that the LAT:Grb2:SOS networked assembly has the dynamical structure of a loosely entangled polymer.

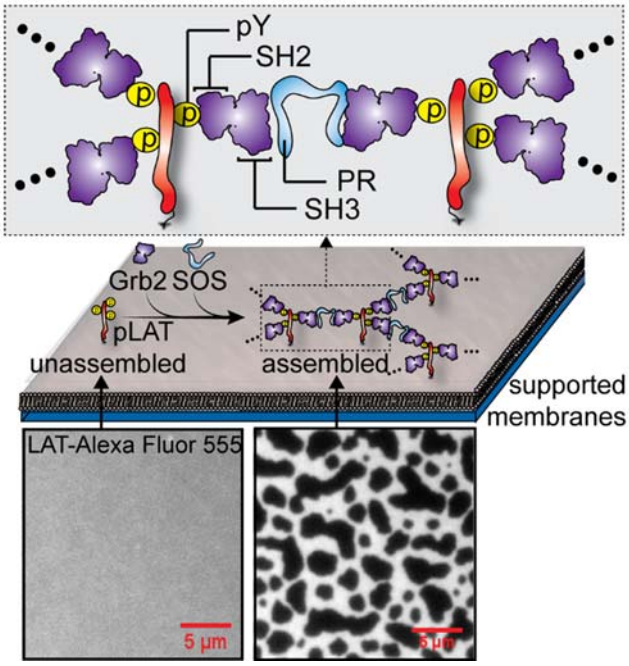

Fig. 4-6 Molecular assembly of LAT:Grb2:SOS by bond percolation. These bonds are transient and reversible modular protein-protein interactions (inset). Membrane-anchored LAT are crosslinked by membrane-recruited cytosolic proteins, Grb2 and SOS. The probability of crosslinking adjacent LAT is determined by the binding kinetics between each molecular species. The dissociation constants of SH2:pY and SH3:PR (proline-rich domain) are about 300 and 400 nM, respectively(1). In the reconstitution experiments, addition of Grb2 and SOS in solution drives assemblies with pLAT on supported membranes. The images of fluorescently labeled LAT (Alexa Fluor 555) are shown before (bottom, left) and after (bottom, right) assembly.

We reconstitute the LAT:Grb2:SOS assembly on supported membranes using the cytoplasmic domain (residues 30 to 233) of LAT with an N-terminus 6-His tag, which was chelated onto DOPC bilayers containing 4% Ni-NTA lipids (Fig. 4-6) (13, 24). Typical LAT densities on the membrane surface for these experiments, measured by fluorescence correlation spectroscopy (FCS) (58), were ~2,400 molecule/μm^2. LAT was phosphorylated by inclusion of dilute Src family kinase, Hck, on membranes (typically with densities of < 100 molecule/μm^2). No phosphatase was included in these experiments, thus we expect LAT to be fully phosphorylated. Under these experimental circumstances, Hck kinase activity is indistinguishable from Zap70, and corresponds to the physiological situation of strong receptor activation (13). Single-molecule trajectories from individual LAT molecules were tracked by labeling a trace fraction (~0.1%) with Alexa Fluor 555 fluorescent dye and imaging on a total internal reflection fluorescence (TIRF) microscopy setup.

In the absence of assembly, single-molecule trajectories of LAT on the supported membrane reveal simple diffusive motion, with a linear scaling of mean-squared displacement (MSD) with time (Fig. 4-7A). MSD analysis is performed on each time trajectory of positions, $\{x(t), y(t)\}$, by the time-averaging protocol: $(n\delta t) = \frac{1}{N-n-1}\sum_{j=1}^{N-n-1}\{[x(j\delta t + n\delta t) - x(j\delta t)]^2 + [y(j\delta t + n\delta t) - y(j\delta t)]^2\}$, where δt is the time between frames, N is the total number of frames in a single trajectory, and n and j are positive integers (59). MSD traces from single trajectories greater than 100 frames were analyzed in terms of a power law, $MSD(t) = At^k$. For unassembled LAT on the supported membrane, fitted values of k were around unity over all timescales, indicating simple Brownian motion. In this case, the diffusion coefficient (D) is well defined and $A = 4D$ for two-dimensional motion. Fit values of D were around 1 - 1.5 μm^2/s (Fig. 4-7B), which are typical for a monomeric protein on supported membranes (25, 60).

To trigger networked assembly of LAT, Grb2 and the proline-rich domain of SOS where added in the solution at 5.8 and 1.45 μM, respectively. Under these conditions, an extended LAT:Grb2:SOS network assembles over the course of about 30 min, after which the system reaches a semi-stationary state (Fig. 4-7A). Single molecule LAT trajectories were analyzed from this semi-stationary state.

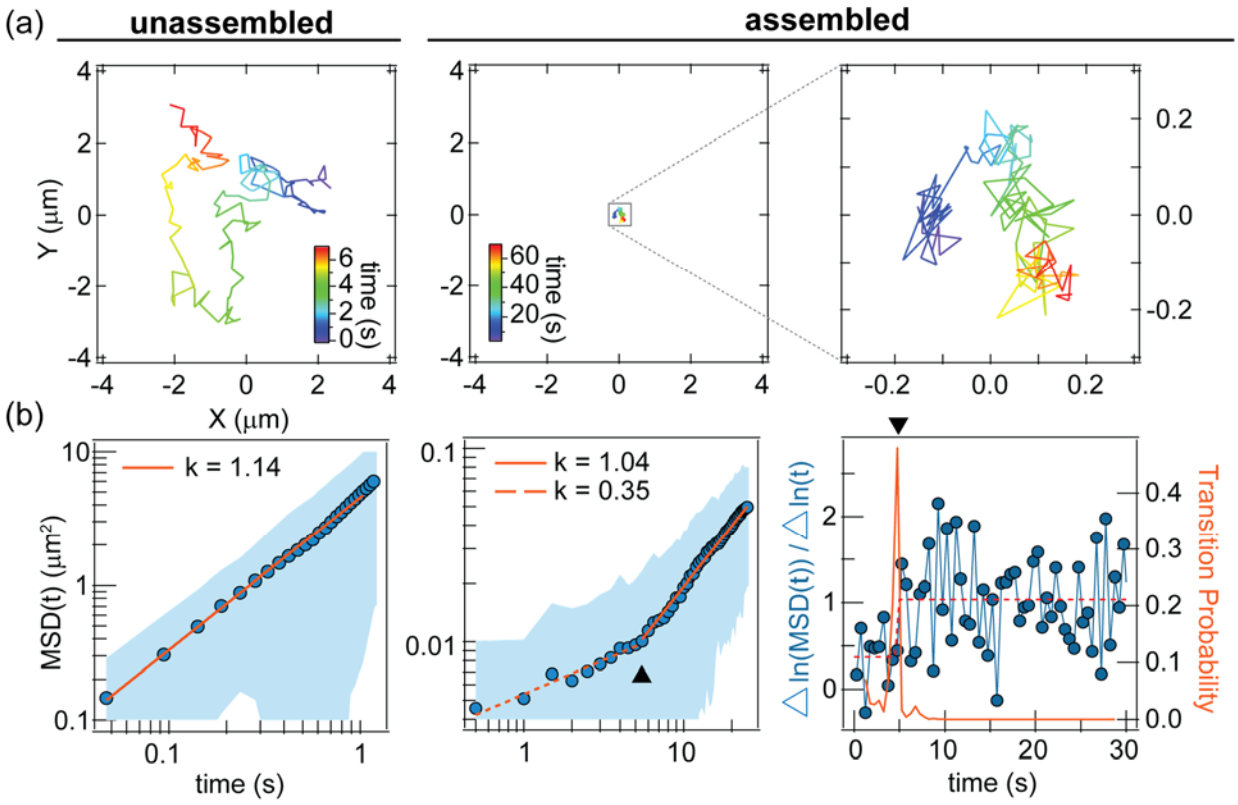

Fig. 4-7 Dynamic scaling of LAT:Grb2:SOS assembly. (a) Single-molecule tracking of LAT before and after assembly. The time axis is color coded in the trajectory. (c) Time-averaging MSD analysis for the trajectory in (a), fitted to a power law in log-log plot. The fitted A for $k = 1.14, 1.04, 0.35$ are 4.5, 0.0017, and 0.0054, respectively. Shaded area are the standard deviation of statistics from a single trajectory. The characteristic timescale (triangle) is estimated with a Bayesian change-point algorithm (right).

Single-molecule imaging of LAT in the assembled state, acquired at a relatively slow framerate of 2 Hz, reveals highly constrained and localized motion (Fig. 4-7A). This slow acquisition strategy allows individual molecules to be tracked for hundreds of seconds prior to photobleaching. MSD analysis shows that below a characteristic timescale of a few seconds, LAT is subdiffusive ($k \sim 0.1 - 0.4$). Over longer time intervals, linear scaling of MSD with time ($k \to 1$) is restored, albeit with slow diffusion coefficients of < 0.01 μm^2/s (Fig. 4-7B). The characteristic timescale is determined using a Bayesian change-point algorithm and a threshold Bayes factor of 3 for substantial evidence of a transition occurring within the trajectory(50) (Fig. 4-7B). Observations over many trajectories confirm that the transition between subdiffusive and normally diffusive motion exists in the time domain only, all tracked molecules reside within the LAT gel and mobility is spatially homogeneous. Membrane-bound Grb2 and SOS also exhibit similar transitions from subdiffusive to diffusive dynamics on short time scales. Errors from tracking due to instrument stability and the tracking algorithm are assessed using LAT molecules immobilized directly on glass surfaces. Immobile molecules result in weak power dependence ($k \ll 0.1$) and absence of a characteristic transition timescale within hundreds of seconds. Therefore, we conclude that the measured trajectories are dominated by genuine molecular motion.

Next, we discuss the physical origin of the subdiffusive motion with Monte Carlo simulations of random walks on a two-dimensional lattice geometry. Specifically, we verify how each mechanism manifest themselves in time-averaging MSD curves identical to the SMT analysis. Firstly, we consider three classes of subdiffusion mechanisms: ***i***) polymer constraints, ***ii***) confinement from compartmentalization and, ***iii***) crowding effects. A purely random walk on a lattice yields a scaling of $k \to 1$ (Fig. 4-8A). Simple polymer constraints (49, 61, 62) recreates subdiffusive motion over short timescales while diffusive motion is observed on longer timescales (Fig. 4-8A). Confinement by an impassable square box results in a plateau in the MSD curve (Fig. 4-8B). Crowding effects are considered by trapping of molecules with a heavy-tail

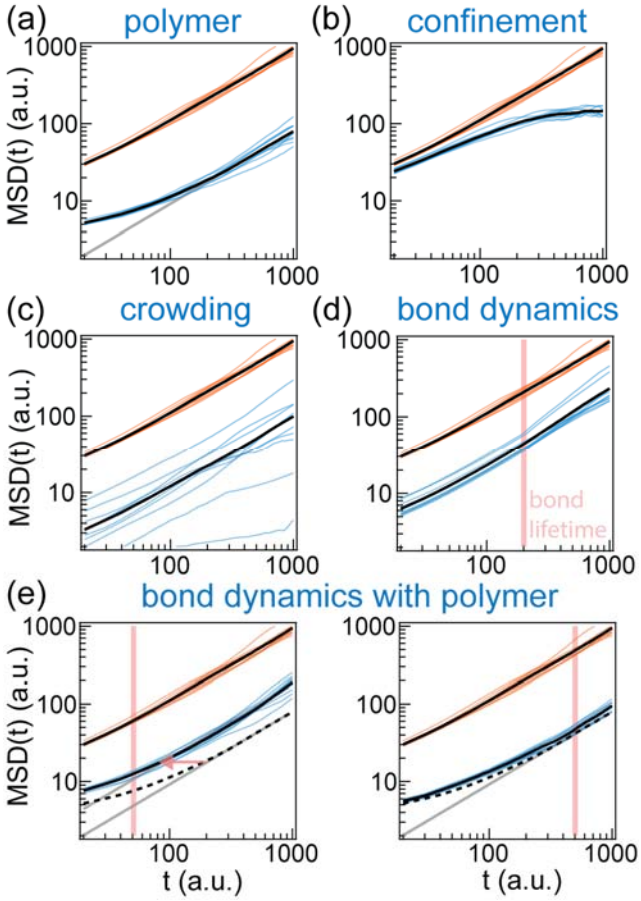

Fig. 4-8 Time-averaging MSD from Monte Carlo simulations of 2D random walk. Molecular motions are constrained by (a) polymer bonding, (b) confinement, (c) crowding effects, (d) bonding to immobile sites and, (e) bonding to polymer. Orange and blue curves correspond to 10 simulated trajectories by Brownian and labeled mechanism, respectively. Black curves are the averaged values. Grey curves are guideline for linear scaling of MSD with time. Dash lines are reference to polymer constraints. Red lines denote the lifetime of bonding to a polymer. In (c) and (d), the MSD for the associated mechanisms are multiply by a factor of 10 for clarity.

waiting time. In this case, the ensemble MSD follows subdiffusion while MSD from individual trajectories does not exhibit subdiffusion (Fig. 4-8C) (63, 64). While there are multiple mechanisms that may lead to crowding effects on dynamics, these typically generate time-independent diffusive or subdiffusive MSD curves, without distinct transitions (65). Therefore, the observed dynamical scaling law of LAT mobility within the condensed assembly is most consistent with the viscoelastic motion of a polymer.

The LAT:Grb2:SOS assembly does not form a conventional polymer. It differs by the fact that individual bonds are rapidly forming and breaking and some of the system dynamics result from these bond rearrangements. The bond dynamics themselves will increase the overall molecular turnover within the system as individual molecules may join and exit the assembly or move within it via a bind-unbind-rebind mechanism. However, bond dynamics alone, without polymer motion, does not reproduce subdiffusion (Fig. 4-8D). Bonding to and escaping from a dynamic polymer network recreate the time-dependent subdiffusion with increased mobility, yet the bond lifetimes may truncate the transition timescales from polymer constraints if they are sufficiently short (Fig. 4-8E). Nevertheless, the net effective bond lifetime of a LAT bonding to an assembly network depends on simultaneous breakage of all three linkages (Fig. 4-6), which is estimated to be much greater than 10 s (13). Given that the transition timescales of LAT assemblies are all within 10 s, these observed timescales are mostly attribute to polymer dynamics, while bond rearrangements may facilitate their mobility. This is further supported by the observation that Grb2 and SOS trajectories (which are terminated when the molecule escapes the assembly) both show similar characteristic timescales. Collectively, the measured dynamics of the overall system follow the behavior of a polymer. Additional features of the LAT assembly structure can be resolved by imaging at faster frame rates.

(a)

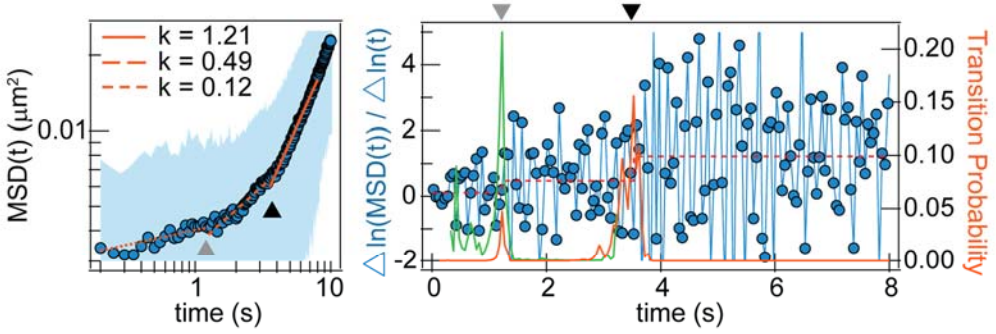

(b)

The reptation model		observed characteristic timescales
The reptation time	$\tau_{rep} = \tau_0 N_e^2 (N/N_e)^3$	5.1 ± 3.2 s
The Rouse time	$\tau_R = \tau_0 N^2$	1.2 ± 1.2 s
The Rouse time for an entangled strand	$\tau_e = \tau_0 N_e^2$	not observed (< 100 ms)

Fig. 4-9 Multiple subdiffusive timescale. (a) MSD analysis of LAT mobility acquired at a framerate of 21 Hz. Each timescale is fitted by a power law, with the characteristic timescales denoted by triangles. The orange and green curve of the right plot corresponds to the transition probability calculated from the full timescale and the partial timescale prior to the slower (black triangle) characteristic timescale, respectively. (b) Comparison of the relaxation timescales between SMT and the reptation model. τ_0 is the relaxation time of a monomer. ± denotes the standard deviations.

In experimental trajectories imaged at a 21 Hz frame rate, multiple relaxation timescales can be resolved for LAT motion within the assembly ($k_1 \sim 0.1, k_2 \sim 0.4$) (Fig. 4-9). This provides evidence for effective entanglement. The viscoelastic motion of a polymer arises from its relaxation modes, first analytically calculated by Rouse (49, 66) and expanded to entangled polymers by De Gennes (49, 67). The reptation model for entangled polymers predicts multiple timescales of subdiffusion due to neighboring bond and topological constraints. In order of increasing timescale, these can be broken down as the Rouse time of an entangled strand (τ_e), the Rouse time (τ_R), and the reptation time (τ_{rep}). Comparison between the reptation model(49) and LAT assembly is summarized in Fig. 4-9B. Assignment of the observed timescales to the model is established by first recognizing that only the reptation time exhibits a temporal transition from subdiffusive to diffusive motion, while the Rouse time defines a transition between subdiffusive motions with different characteristic scaling. The observed scaling also follows the prediction of the reptation model ($k_{t>\tau_{rep}} > k_{\tau_{rep}>t>\tau_R} > k_{\tau_R>t>\tau_e}$).

For an ideal polymer, the timescale of relaxation is determined by the longest relaxation mode, which reflects the total size and entanglement of the polymer strand. Within the 38 by 38 μm field of view, the distribution of observed relaxation timescales for individual trajectories within the LAT assembly is broad ($\tau_{rep} = 5.1 \pm 3.2, \tau_R = 1.2 \pm 1.2$ s) (Fig. 4-9B). In some trajectories, subdiffusion persists without a characteristic transition timescale, indicating the existence of larger local assemblies. LAT assemblies of different sizes evidently coexist. Averaging the statistics provides estimations about the mean extent of connectivity within the assembly. The relative size of entanglement, N/N_e where N_e is number of monomers in an entangled strand and N is the total number of monomers in the polymer, is about 4-5 for LAT assembly, suggesting a rather loose entanglement. The unobserved τ_e is estimated to be 10-100 ms, which is at the limits of the instrument resolution.

Given a minimum multivalency of three, LAT can form macroscopic assembly network if the bonding probability (p) between adjacent LAT (e.g. through the LAT:Grb2:SOS:Grb2:LAT motif) exceeds the critical threshold ($p_c = \frac{1}{f-1}$ where f is the multivalency). Based on these considerations, a bond percolation model for the LAT:Grb2:SOS assembly is generated in Fig. 4-10. Qualitatively, entanglement of large polymers is prominent near or above the gel point; this condition is achieved in the reconstituted experiments.

In summary, SMT of LAT within the phosphotyrosine-mediated assembly reveals a dynamic scaling law similar to that of an entangled polymer. Thus although the assembly is distinct from a classical polymer in that all of its individual bonds are rapidly breaking and reforming, the mean connectivity within the structure still manifests in a characteristic dynamical scaling law. Furthermore, these dynamical features are different from a viscous fluid. In living cells, subdiffusive motion is commonly observed and often attributed to confinement and crowding effects (43, 68). Here, we demonstrate that organization of proteins into networked assemblies leads to timescale-dependent subdiffusion. Moreover, this type of analysis could be performed in live cells (6, 43), providing a way of characterizing the molecular-scale organization of visible signaling structures based on dynamics.

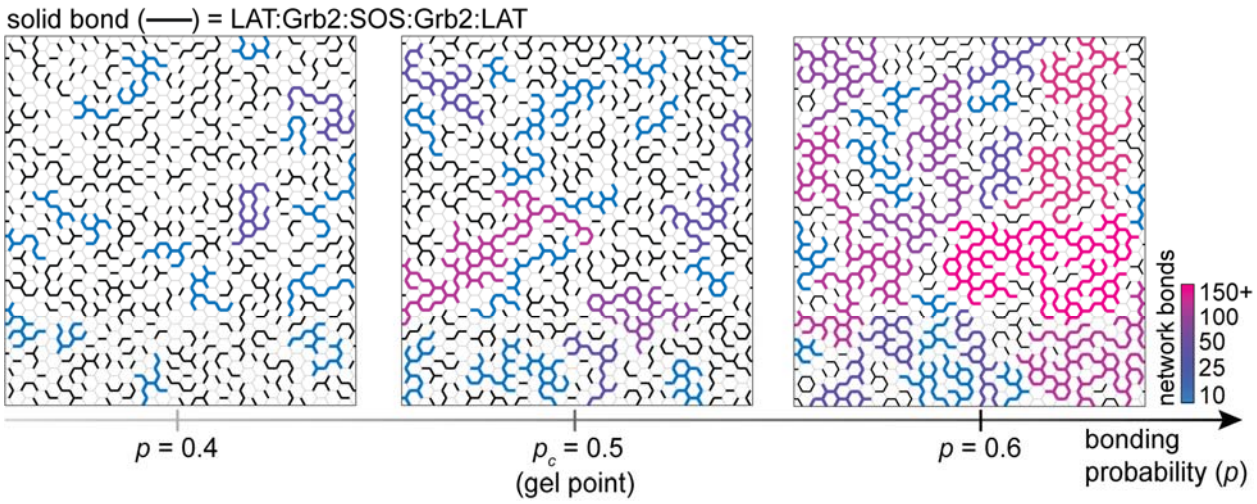

Fig. 4-10 A bond percolation model for LAT assembly. LAT has a multivalency of three, which is represented by honeycomb lattices. Each intersection represents a LAT molecule, while each edge represents a possible bond of LAT:Grb2:SOS:Grb2:LAT with a bonding probability (p). Black and grey bonds denote bonding and non-bonding interactions, respectively. The color gradient represents network sizes that are greater than 10 bonds.

Part II. Catalysis on membranes

5. Enzymatic catalysis on membrane surfaces

Enzymatic reactions and subsequent protein binding to enzymatically-modified proteins constitute the primary mechanism of signal transduction in living systems[5]. The physical mechanism and rates of catalysis can not only enhance or attenuate the response time of a signaling system, but can alter the qualitative shape of the input-output function of a signaling cascade (69). Many substrates in different signaling pathways, such as the T-cell receptor (TCR), epidermal growth factor receptor (EGFR), linker for activation of T cells (LAT), nephrin, and programmed cell death protein 1 (PD-1), contain repetitive, modifiable motifs (7, 10, 69). Furthermore, the degree of multivalency, phosphorylation dynamics, and how proteins interact with the modified substrate are intimately relevant to how signals are relayed in a signaling cascade; especially in light of recent evidence that many of these receptors form molecular assemblies after phosphorylation (13, 30, 55).

Another common feature of these signaling receptors is that they reside on the plasma membranes during phosphorylation. Membranes alter many facets of reaction kinetics, including reduced dimensionality, constrained orientation and accessibility to the substrates (2, 11, 25). Hence, the native membrane signaling geometry is inherently coupled to the phosphorylation kinetics and how their binding partners interact with these receptors (70, 71). Therefore, to properly understand signal transduction on membranes, quantitative measurement of enzymatic reaction kinetics and assessment of protein-protein interactions on membranes is necessary, especially from a modeling perspective (9). Unfortunately, direct enzymatic reaction and protein-protein binding measurements on membranes are often hindered by the intrinsic challenges of performing quantitative experiments on membranes. In addition, reaction rates measured in solution cannot be easily translated to that on membranes because conversion of dimensionality does not account for translational and rotational constraints, conformational changes, and accessibility constraints on membranes (2). Most catalytic measurements on membranes are *ad hoc*, and only can report catalytic rates instead of the rate constants. In this chapter, we report a substantial difference

[5] Contents in this chapter are in manuscript preparation (W.Y.C. Huang*, J. Ditlev*, H.-K. Chiang, M.K. Rosen, J.T. Groves, * denotes equal contributions)

between solution-based and membrane-based Grb2 binding to phosphotyrosine residues on LAT as well as phosphorylation kinetics of LAT by ZAP-70 using a 2D enzymatic assay on supported membranes. Our results demonstrate the necessity to properly analyze membrane-associated reactions using two-dimensional assays that can assess binding and enzymatic reactions in the proper experimental geometry.

In vitro reconstitution of LAT phosphorylation by ZAP-70

In our 2D enzymatic assay on supported membranes, ZAP-70 is recruited to a pre-phosphorylated cytoplasmic domain of CD3 ζ chain (pCD3) where it can phosphorylate its substrate LAT (Fig. 5-1A). Both pCD3 and LAT are chelated onto DOPC bilayers containing 4% NiNTA-modified lipids (24). The densities of laterally fluid LAT can be controlled from 50 to 3000 molecule/μm^2 (covering physiological densities of 100-1000 molecule/μm^2) and were measured by fluorescence correlation spectroscopy (FCS). The phosphorylation of LAT by ZAP-70 was probed via Grb2 recruitment in real time. Grb2 contains one SH2 domain that binds to phospho-LAT (pLAT) with fast binding kinetics (~500 ms) (13), making it an ideal candidate to measure LAT phosphorylation. To enhance the resolution of phosphorylation detection and to avoid futile phosphorylation events, LAT was specifically engineered to preserve only the four distal tyrosines (Y) (LAT4Y). These four tyrosines have been identified to play the most critical role during T-cell activation. Three of the most distal tyrosines (Y171, Y191, Y226) are known to have high affinity with Grb2, while Y132 recruits phospholipase PLCγ (22).

The assay was then optimized for the following kinetic considerations to resolve phosphorylation: ***i)*** Grb2 rapidly reports phosphorylation (< 1 s), ***ii)*** ZAP-70 is recruited to membranes by pCD3 at a moderate rate (~60 s) and, ***iii)*** phosphorylation occurs at a slow rate (~10 min) (Fig. 5-1B). ***(i)*** and ***(ii)*** has lower limits defined by the binding kinetics of the ligand-receptor pair. In our experiments, injection of 500 pM ZAP-70 and 50 nM Grb2 onto a bilayers containing pCD3 of ~500 molecule/μm^2 and LAT of 50-2000 molecule/μm^2 satisfies these conditions. At this Grb2 concentration, it acts as a phosphorylation sensor by stochastically sampling the pY of membrane surfaces rapidly

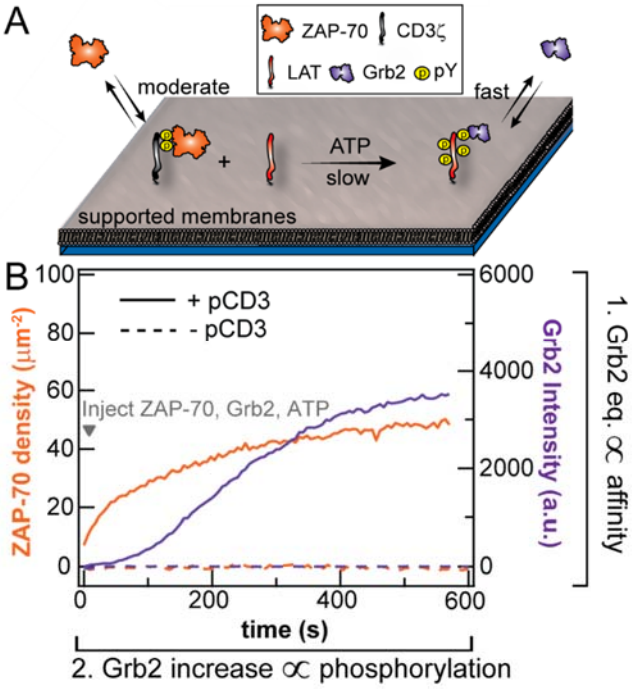

Fig. 5-1 Reconstitution of LAT phosphorylation by ZAP-70 (A) Biochemical reconstitution of LAT phosphorylation by ZAP-70 on supported membranes. LAT and pCD3 are tethered onto fluid bilayers. ZAP-70, Grb2, and ATP are injected into the solution to monitor phosphorylation. (B) Simultaneous imaging of ZAP-70-Alexa Fluor 488 and Grb2-Alexa Fluor 647 during phosphorylation. The initial increase and final equilibrium phase of Grb2 reflects the ZAP-70:LAT phosphorylation and LAT:Grb2 affinity, respectively.

(< 1 s) without saturating all the pY, i.e. each LAT4Y has less than one Grb2 bound on average. Fluorescent labeling of ZAP-70 and Grb2 with Alexa Fluor 488 and Alexa Fluor 647, respectively, allows simultaneous imaging of the membrane-bound components using total internal reflection (TIRF) microscopy. A typical kinetic trace showing ZAP-70 and Grb2 recruitment to the membrane is reported in Fig. 5-1B. The Grb2 intensity trajectory consists of two phases: ***i)*** ZAP-70 recruitment leading to LAT phosphorylation and, ***ii)*** equilibrium of Grb2 with fully phosphorylated LAT. The increase and plateau of Grb2 intensity reflects LAT phosphorylation and LAT:Grb2 affinity, respectively. Phosphorylation by solution ZAP-70 is extremely slow in this experimental condition (>> 30 min), confirmed by the negligible phosphorylation rate of LAT by ZAP-70 without pCD3 (Fig. 5-1B). To properly extract the phosphorylation rate on membranes, we first require an understanding of how Grb2 binds to the multivalent pY of LAT.

Multivalent cooperativity in the LAT:Grb2 binding kinetics

The affinity of each LAT tyrosine to Grb2 was first deconstructed by measuring the binding kinetics with monovalent LAT mutants. Solution isothermal titration calorimetry (iTC) of different pairs of monovalent LAT:Grb2 shows similar affinity trend (K_A^{sol} : LATFFYF:Grb2 > LATFYFF:Grb2 ≈ LATFFFY:Grb2) with previous studies (22), albeit with overall lower K_A (Table 5-1), presumably due to reduced accessibility for full length LAT. LATYFFF:Grb2 has a low affinity that is below the instrument resolution, consistent with previous study (22). (For our notations, the tyrosine mutations of LAT are implicitly Y132-Y171-Y191-Y226, e.g. LATFFYF is LAT-Y132F-Y171F-Y226F).

Next, the affinity of each LAT:Grb2 pair were measured on supported membranes (Fig. 5-2A). On membrane surfaces, two unpredicted results are observed. First, the affinity trend is reversed compared to solution iTC (K_A^{mem} : LATFFYF:Grb2 < LATFYFF:Grb2 < LATFFFY:Grb2) (Fig. 5-2B). Single-molecule dwell time analysis shows that the off rates are similar for all monovalent LAT:Grb2 pairs (Fig. 5-3), suggesting that the on rates, hence geometric accessibility, regulate their affinity. Second, the affinity of LAT4Y:Grb2 cannot be linearly reconstructed by monovalent LAT mutants (Fig. 5-2B), i.e. having the four tyrosines on the same LAT molecule has about 4-5 fold increase in affinity. Furthermore, we compared the affinity between LAT4Y:Grb2 and trivalent LAT:Grb2 (Fig. 5-2C). In these experiments, deletion of Y132 (which does not recruit Grb2 by itself, Fig. 2B) reduces the affinity of other tyrosines to Grb2 (Fig. 5-2C). The cooperativity in LAT:Grb2 affinity is summarized in Fig. 5-2D. Because each LAT:Grb2 pair have similar off rates, affinity cooperativity from multisite regulation is attributed to the on rates (Fig. 5-3), suggesting that the degree of phosphorylation may mediate a structural orientation of full length LAT on membrane surfaces, even though the protein has no known structure. Dwell time analysis also eliminates Grb2 hopping between pY residues on LAT as a rebinding

LAT1Y Variant	K_D (nM)	ΔH (kcal/mol)	ΔS (kcal/mol·K)
LAT FFFY	458.9 (320, 668)	-13.8 (-15.22, -12.67)	-18.1
LAT FFYF	195.0 (134, 281)	-15.0 (-16.36, -13.91)	-20.5
LAT FYFF	462.9 (331, 669)	-15.0 (-16.31, -13.77)	-22.0
LAT YFFF	N.A.	N.A.	N.A.

Table 5-1 Solution-based isothermal titration calorimetry of monovalent LAT:Grb2

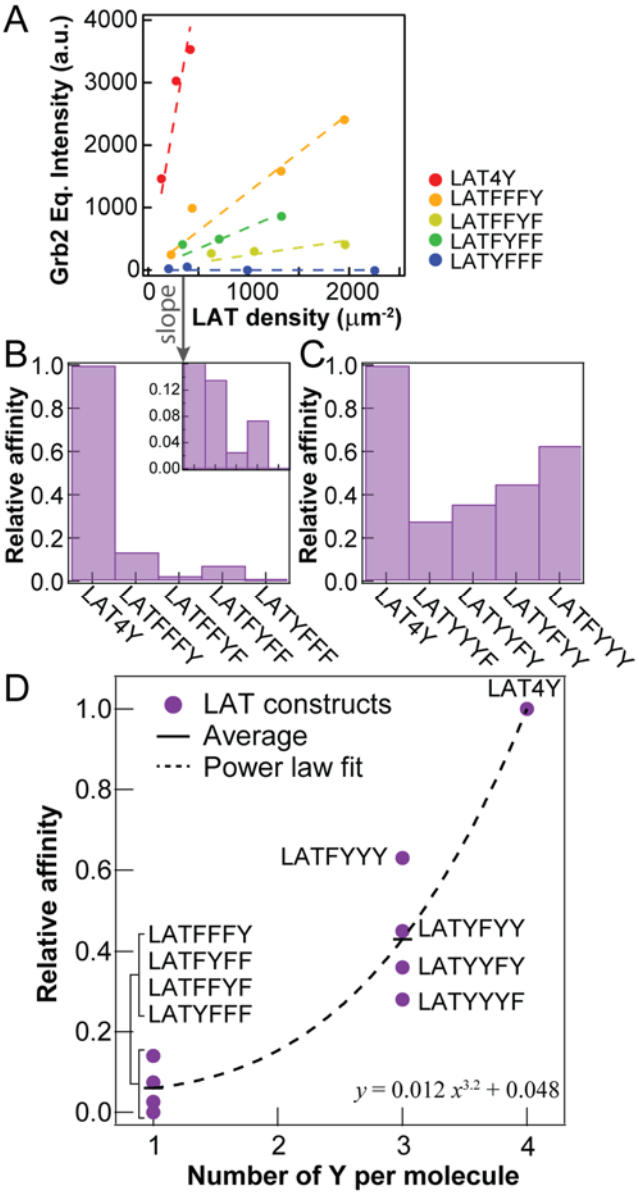

Fig. 5-2 Multisite cooperativity in pY:Grb2 affinity (A) Grb2 equilibrium point from LAT density titration. (B) Comparison of the slope in (A) provides relative affinity between monovalent LAT constructs to Grb2. (C) Relative affinity for trivalent LAT. (D) Summary of (B) and (C). Power law fit is an empirical fit.

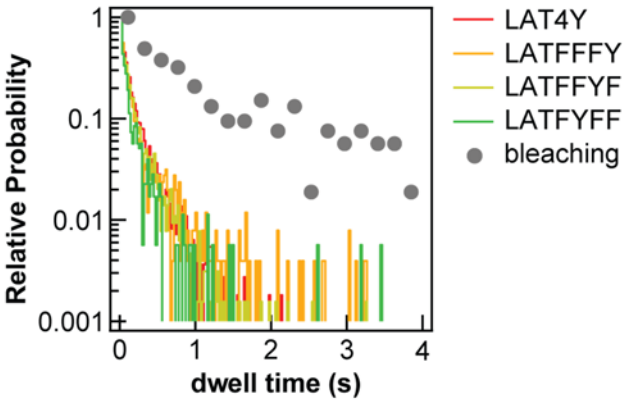

Fig. 5-3 Grb2 exhibits similar off rate for different LAT constructs. Dwell time distributions from single-molecule tracking. Bleaching curve (grey) is the dwell times for immobilized LAT on a glass substrate.

mechanism in the reconstitution experiment. We further confirm that the imaging experiments are not related to difference in photophysics of the dye for different LAT constructs, as evident from the brightness analysis from FCS and fluorescent lifetime analysis. Conceivably, this cooperative affinity enhances the sensitivity of Grb2 recruitment during cellular signaling.

Determining catalytic rate constants from enzymatic trajectories

To obtain the catalytic rate constants of LAT phosphorylation, phosphorylation rates were measured as a function of LAT density (Fig. 5-4A). To account for protein copy number of recruited ZAP-70, the data were analyzed according to the following equation:

$$v(t) = \frac{1}{E(t)} \frac{dP(t)}{dt} \qquad [5.1]$$

where v is the initial rate of phosphorylation, E is the ZAP-70 density on membranes, and P is the pLAT density inferred from Grb2 recruitment. For simple Michaelis–Menten kinetics, $v = \frac{k_{cat}[S]}{K_M+[S]}$ where k_{cat} is the catalytic rate and K_M is the the Michaelis constant. The raw linear initial rates for phosphorylation of LAT4Y and monovalent LAT are summarized in Fig. 5-4B. Finally, the rate constants are obtained by calibrating the affinity for each LAT:Grb2 pair (Fig. 5-2 and 5-4C). For monovalent LAT phosphorylation, the rate constants are about 5×10^{-5} $\mu m^2 s^{-1}$ (Table 5-2). Note that the assay naturally produces proper 2D units for the rate constants. The initial rates in these cases are approximately linear, suggesting that catalysis are near a diffusion-limited region.

The case for LAT4Y phosphorylation requires consideration of phosphorylation mechanism due to multivalency. Processive catalysis is a modification mechanism in which multiple phosphorylation can take place per encounter between the enzyme and the substrate (72). It has been speculated that kinases or phosphatases in the TCR activation pathway exhibit processivity due to the prevalence of multivalent substrates. Experimental verification of this mechanism is compounded by the fact that processivity is intimately related to the diffusion of the molecules (73). In our reconstituted experiments, the type of phosphorylation mechanism will affect reconstruction of the phosphorylation rate constants since the conversion of Grb2 readout to tyrosine densities will scale nonlinearly due to cooperative affinity. However, the following self-consistency analysis, with the monovalent LAT as a benchmark, can be informative:

$$\text{reconstructed LAT4Y phos. rate } (f) = f \times \text{monovalent LAT avg. phos. rate} \qquad [5.2]$$

where f is the degree of processivity, ranging from 1-4 in the case of LAT4Y. Only moderate processive mechanism ($f = 2.4$) satisfies this self-consistency, both purely distributive ($f = 1$) and strong processive ($f = 4$) mechanism are not self-consistent (Fig. 5-4C).

Discussion

Membranes modulate biochemical reactions by requiring dimensional constraints, alteration of accessibility, and reduction of diffusion. The first two factors play an unexpected effect on modulating LAT:Grb2 binding kinetics, providing cooperativity by means of on rates. Diffusion defines the asymptotic rate for an efficient enzymatic reaction. The linear initial rates of LAT4Y phosphorylation in the titrated densities suggest that catalysis on membranes is seldom saturated by substrates and operates near a diffusion-limited regime (a high K_M density). The net effect of membranes can be estimated by comparison with phosphorylation rate of LAT peptide by ZAP-70 in solution: simple dimensional conversion of solution catalytic rate constants to 2D is about 5×10^{-3} $\mu m^2 s^{-1}$, close to two order of magnitude faster than the membrane measurement.

In conclusion, we established a kinetic assay that resolves enzymatic rates on a 2D geometry. The necessity of membrane reconstitution approach is reinforced by several observations that physical properties of membranes alter the binding kinetics and enzymology of biochemical reactions. While the assay is performed with receptor-recruited cytosolic kinase, activity of membrane-bound kinases or phosphatases, such as Lck or CD45, could be measured in a straightforward manner.

This assay quantitatively addresses enzymology on membrane surfaces, and evaluates their contributions to biochemical networks.

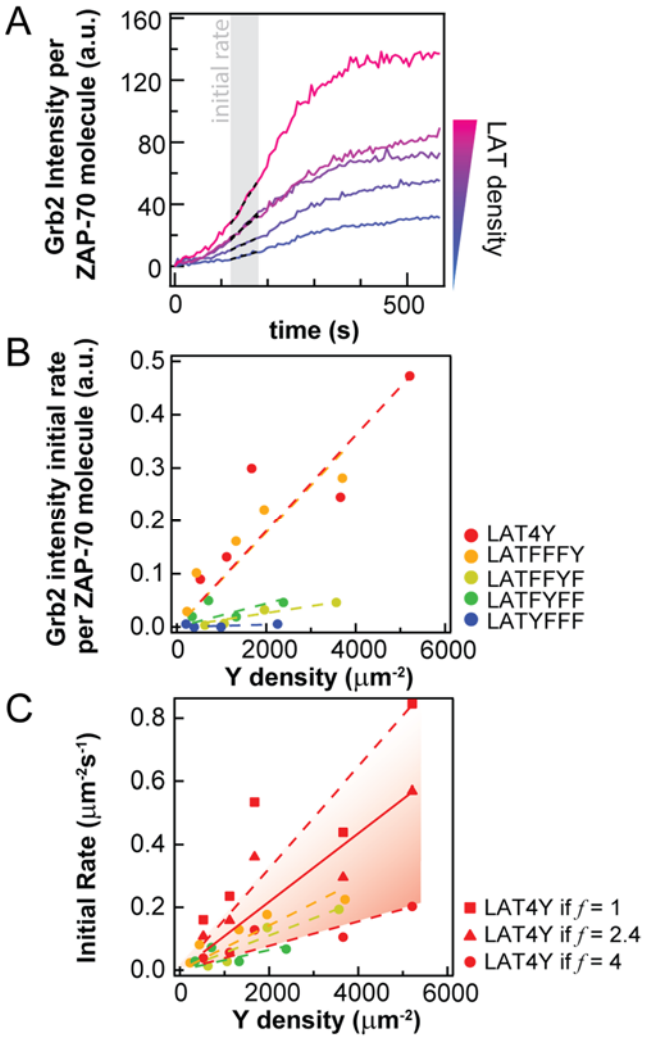

Fig. 5-4 2D enzymatic analysis (A) The apparent initial rates are obtained from linear fitting of Grb2 intensity from LAT density titrations. (B) The apparent initial rates from (A). (C) The effective catalytic rate in proper 2D units, after correction of affinity (Fig. 2D). The rate constants are summarized in Table 2. Shaded area are possible rate constants region with dark gradient indicating higher processivity. The red dash lines correspond to purely distributive or strong processive mechanism. The red solid line denotes self-consistent solution to Eq. (2). Distributive mechanism leads to higher apparent rate than processive mechanism because the increase of Grb2 signals corresponds to more phosphorylation events by considering the cooperative affinity.

LAT constructs	**Effective catalytic rate constant ($\times 10^{-5} \cdot \mu m^2 s^{-1}$)**
LAT4Y (f = 2.1)	10.9
LATFFFY	7.1
LATFFYF	5.5
LATFYFF	3.2
LATYFFF	N.A.

Table 5-2 Rate constants of LAT phosphorylation by ZAP-70

6. Molecular configurations and catalysis

Oligomerizations of cytosolic enzymes on membranes through protein-protein or lipid-protein interactions is a recurring theme in signal transduction[6] (74). Some examples include dimers such as Raf-1 (75) or larger assembly such as LAT:Grb2:SOS (13, 55) described earlier. While the elongation of dwell times through extended complex affects the overall turnover, it remains to be examined whether the fundamental bimolecular catalytic rate depends on the oligomerization itself. Conceivably, molecular structure on membranes can modulate catalytic rate by changing the probability of encounter between the enzyme and the substrate. Thereby, molecular configurations can be intimately linked to the potency, or even specificity, of signal reactions.

In the following example, we briefly illustrate the simplest multivalent membrane receptor with a multivalency of two, programmed cell death-1 (PD-1), binding with the cytosolic phosphatase SHP-2. PD-1 has two phosphotyrosines that bind to the tandem SH2 domains of SHP-2. It is often assumed that both of the SH2 domains binds to the same PD-1, thereby enhancing the dwell times nonlinearly via this tandem binding state. However, it is plausibly that a multivalency of two may result in a crossing linking conformation that bridges different PD-1 molecule together, forming dimers or even higher oligomers. Opposing these states is the condition where saturating amount of SH-2 is presence such that only one of the SH2 domain is binding to PD-1, which we termed as the monomeric binding. The interplay between these conformations affects the dynamical parameters of the recruited SHP-2, such as diffusivity and dwell times. Preliminary single-molecule tracking of SHP-2 at different regions of the phase space defined by the SHP-2 concentrations and PD-1 densities shows that both the diffusion and dwell times of SHP-2 are dependent on the parameters of the phase space (data not shown). Therefore, we first establish a simple equilibrium model to predict the interplay between these molecular configurations.

The model is depicted in Fig. 6-1. We consider the regime of low to intermediate concentrations such that large molecular assemblies are not substantial. The equilibrium fraction of each states are described by the following relations:

[6] Contents in this chapter are in manuscript preparation (W.Y.C. Huang*, E. Hui*, H.-K. Chiang, R.D. Vale, J.T. Groves, * denotes equal contributions)

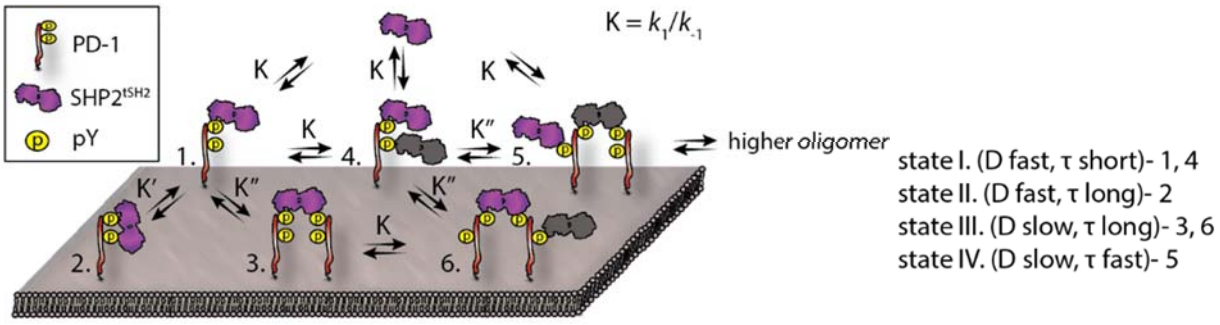

Fig. 6-1 Molecular configurations of PD-1:SHP-2.

$$x_T = x + x_1 + x_2 + x_3 + x_4 + x_5$$

$$x = x_1/KC$$

$$x_2 = K'x_1$$

$$x_3 = K''x_1^2/KC$$

$$x_4 = KCx_1$$

$$x_5 = K''x_1^2$$

where x_i describes the density of i state defined in Fig. 6-1 on membranes, x is the free PD-1, x_T is the total density of all PD-1 and K is the equilibrium constants, and C is the SHP-2 concentration.

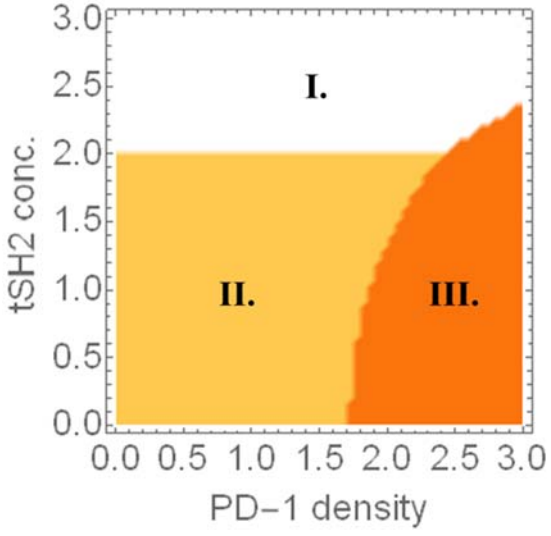

Fig. 6-2 Phase diagram of PD-1:SHP-2 configurations.

Solving the conservation of molecules gives: $x_1 = (\sqrt{b^2 + 4c} - b)/2$, where $b = \frac{1+KC+K'KC+(KC)^2}{K''(1+KC)}$ and $c = \frac{KCx_T}{K''(1+KC)}$. This model is convenient to relate to membrane titration experiments (i.e. all molecular species are express as a function of x_T and C.) The dominant molecular species of each titration point of the phase diagram is plotted in Fig. 6-2. Note that the transition in the diagram is in reality continuous. This mapping allows further experimental assay to probe whether catalytic rate is identical within the phase diagram. While this is an ongoing study, we will illustrate one example of the profound effect of molecular configurations and membrane recruitments in determining the outcome of a signal cascade.

7. Geometry sensing from bistable competitive reactions

One important class of membrane constituents that act as master regulators of signal transduction is the large family of phosphatidylinositol (PI) lipids, which selectively recruit cytosolic proteins to intracellular membranes and locally control their activity. PI lipid reactions are regulated by kinase-phosphatase competition that chemically modifies lipid head groups to switch molecules among the various PI phosphate (PIP_x) species. Bistability within these otherwise futile reactions can lead to emergent properties, such as spatial patterning of PI lipids during phagocytosis (76, 77), polarized cell migration (78, 79), pheromone sensing (80, 81), and cytokinesis (82). Spatial self-organization in the distribution of biomolecules is an emergent property of many reaction diffusion systems in biology (83-85).

Here we investigated how spatial order in PtdIns based kinase-phosphatase competition reaction is established, maintained, and influenced by the geometry of the reaction environment. We examine the effects of geometric confinement on the competitive balance between a kinase and opposing phosphatases acting on membrane PIP_x lipids. Controlled geometric confinement of the membrane reaction is achieved using micropatterned supported lipid membranes (26, 86) and membrane coated glass microspheres (87). In both cases the membrane area and shape is precisely controlled, without interfering with membrane lipid mobility, while the adjacent three-dimensional solution (containing the enzymes) remains continuously connected and homogeneous. This system exhibits bistability, with PI(4)P and $PI(4,5)P_2$ dominated states both accessible from the initial conditions. However, we observe that the final outcome depends on the geometric size of the reaction environment, which is not predicted by a macroscopic interpretation of kinetic bistability. In smaller membrane corrals, the $PI(4,5)P_2$ state is favored while in larger regions PI(4)P dominates. Using stochastic kinetic modeling, we demonstrate that the geometric size sensing exhibited by this reaction system stems from an asymmetric response to stochastic composition fluctuations. Strong positive feedback in the kinase reaction, which is not mirrored in the phosphatase, captures positive fluctuations in $PI(4,5)P_2$ composition and takes the system to the $PI(4,5)P_2$ dominated state. This effect is more prominent in smaller reaction systems where intrinsic stochastic composition fluctuations are relatively larger.

Reconstitution of self-organized phosphatidylinositol based competitive reactions with positive feedbacks

In the eukaryotic cells, synthesis of $PI(4,5)P_2$ at the plasma membrane is predominantly controlled by type I phosphatidylinositol-4-phosphate 5-kinases (PI4P5K), which phosphorylates the 5'-hydroxyl of PI(4)P lipids (88). Opposing PI4P5K activity are 5'-phosphatases, which catalyze the dephosphorylation of $PI(4,5)P_2$ into PI(4)P (89). To explore that dynamics and emergent properties of a PI lipid based reaction diffusion systems, we biochemically reconstituted a kinase-phosphatase competition reaction built around the synthesis of PI(4)P and $PI(4,5)P_2$ lipids. Using soluble fluorescently labeled lipid binding domains, DrrA/SidM (90-92) and a PH domain derived from PLCδ (93), we specifically and reversibly monitored PI(4)P and $PI(4,5)P_2$ densities on membrane surfaces, respectively. Single molecule binding-desorption measurements confirm both of these lipid sensors exhibit first-order kinetics with membrane dwell times (τ_1) of 25 ms (Alexa488- PLCδ) and 289 ms (Alexa647-DrrA). With probe concentrations adjusted such that only a minor fraction (< 0.1%) of membrane PI lipid was bound to the probe, we can monitor changes in lipid composition by total internal reflection fluorescence (TIRF) microscopy. This system provides real-time and real-space readout of membrane PIP_x composition with sub-second time resolution and sub-micron spatial resolution.

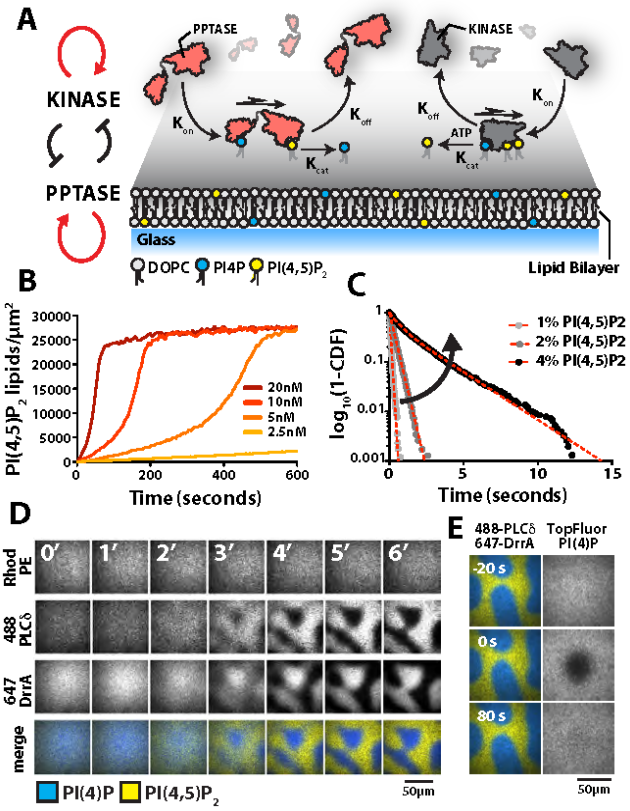

The tendency of a soluble enzyme acting on a membrane substrate to interact with its product leads to positive feedback. In terms of a Michaelis-Menten analogy, additional product binding (independent of the catalytic site) will recruit more enzyme to the membrane as product concentration

Fig. 7-1 Self-organization of a phosphatidylinositol based reaction diffusion system (A) Signaling network architecture of phosphatidylinositol based kinase-phosphatase competition reaction. Lipid modifying enzymes associate with membranes containing a mixture of PtdIns lipids, catalyze reactions, and then dissociate. (B) PI4P5K exhibits intrinsic positive feedback during $PI(4,5)P_2$ synthesis. Synthesis of $PI(4,5)P_2$ was monitor in the presence of 20nM Alexa488-PLCδ. (C) Single molecule dwell time distribution of Alexa647-PI4P5K (1-100pM) measured in the presence of different $PI(4,5)P_2$ lipid densities. (D) Bistable kinase-phosphatase competition reaction drives spatial patterning of PI(4)P and $PI(4,5)P_2$ lipids, but not Rhod PE, on SLBs. Self-organization 10 nM PI4P5K, 17.5 nM DrrA-INPP5E, 20 nM Alexa488-PLCδ, and 20 nM Alexa647-DrrA. Membrane composition: 96% DOPC, 2% PI(4)P, 2% $PI(4,5)P_2$, and 0.001% Rhod PE. (E) PtdIns lipids diffuse across PI(4)P or $PI(4,5)P_2$ lipid domain boundaries unimpeded based on FRAP of TopFluor PI(4)P.

increases (94). This effectively lowers the Michaelis constant, K_M, and increases reaction velocity. Through biochemical characterization of PI4P5K dependent PI(4,5)P_2 lipid synthesis we discovered a positive feedback mechanism intrinsic to PI4P5K (Fig. 7-1B). Single molecule tracking of membrane associated Alexa647-PI4P5K revealed nonlinear changes in k_{off} that were strongly dependent on the density of PI(4,5)P_2 (Fig. 7-1C). In contrast, we found that the 5'-phosphatase domains derived from OCRL and INPP5E catalyzed PI(4)P synthesis with simple bimolecular reaction kinetics. To expand the dynamic range of 5'-phosphatase activities, we engineered positive feedback loops into these simple phosphatase domains. Using these enzymes, we biochemically reconstituted a two-component phosphatidylinositol based kinase-phosphatase reaction diffusion system on a model membrane.

Under conditions that roughly balance the activities of PI4P5K and 5'-phosphatases (simple or engineered chimeras), bistability is observed as the reaction environment splits into regions that are enriched in either PI(4)P or PI(4,5)P_2 (Fig. 7-1D). PI lipid patterns emerge on membranes lacking any pre-existing patterns or positional information. Fluorescently labeled kinase and phosphatase localize to domains enriched in PI(4,5)P_2 and PI(4)P, respectively. The establishment and maintenance of PtdIns lipid domains requires energy in the form of ATP. Varying the total enzyme concentration and kinase-phosphatase ratio modulates the kinetics and surface area of the PI lipid domains. In contrast to the classic Turing system, this bistable PtdIns based reaction diffusion system does not form propagating waves with a discrete periodicity at the approximate steady-state condition. The establishment and maintenance of large-scale PtdIns lipid patterns cannot be described by a phase diagram, is non-conservative, and does not emerge from dynamic instability. Visualizing the bulk localization of rhodamine labeled phosphatidylethanolamine (Rhod PE) lipids demonstrated that only the distribution of the PI lipid phosphorylation state is spatially modulated by the kinase-phosphatase competition reaction; the membrane is otherwise homogeneous and fluid (Fig. 7-1DE).

Bistability of kinase-phosphatase competition reaction

The emergence of spatial heterogeneity in PI lipid composition is definitely linked to the bistable network topology (Fig. 7-1A). However, the appearance of self-organized PI lipid domains did not immediately inform us of their mechanistic origin. For instance, what initially triggers domain formation? We hypothesized that local stochastic fluctuations in PI lipid densities resulting from stochastic membrane binding of enzymes spatially dictates the final outcome of the competition reaction. To eliminate the spatial component and characterize the reaction outcome probabilistically, we reconstituted the bistable kinase-phosphatase competition reaction on two-dimensional membranes partitioned by chromium barriers (Fig. 7-2A). Reconstitution of the competition reaction on 5 μm x 5 μm photolithographically defined membranes resulted in a bifurcation of reaction trajectories, with each corral fluctuating toward one of two stable steady states – predominantly PI(4)P or PI(4,5)P_2 (Fig. 7-2BC). Once an individual corral reached a stable steady state, interconversion of the dominant lipid species was not observed. No long-range communication between neighboring corrals was observed demonstrating that the reactions are restricted to the membrane surface.

The bistable reaction can be described by considering the stochastic chemical kinetics of the competing kinase-phosphatase reactions. In a molecular framework (see *Appendix*), the phosphorylation (J^+) and dephosphorylation (J^-) reactions can be expressed as:

$$J^+ = k_{cat}^+(x_0^+ + x_1^+ + x_2^+)(1-x), \quad J^- = k_{cat}^-(x_0^- + x_1^- + x_2^-)x \qquad [7.1]$$

where $x = \frac{x_{PI(4,5)P2}}{x_{PI(4,5)P2}+x_{PI(4,5)P2}}$ denotes the normalized extent of the reaction defined by the density of PI(4,5)P_2 on membranes, k_{cat} is the effective catalytic parameter, and x_0, x_1, x_2 corresponds to the densities of each molecular species from bimolecular, simple feedback and complex feedback kinetics, respectively (the subscript i in $\underline{x_i}$ denotes the order of reaction on x). For systems that contain at least one nonlinear term, the dx/dt function becomes cubic as a function of x, which has three possible dx/dt = 0 states when reactions are closed to balancing: an unstable state (e.g. x~ 0.5) and two stable steady states (x ~ 0 and x ~ 1) (Fig. 7-2D). Fluctuations near the unstable crossover composition drive the system toward either of the two stable states.

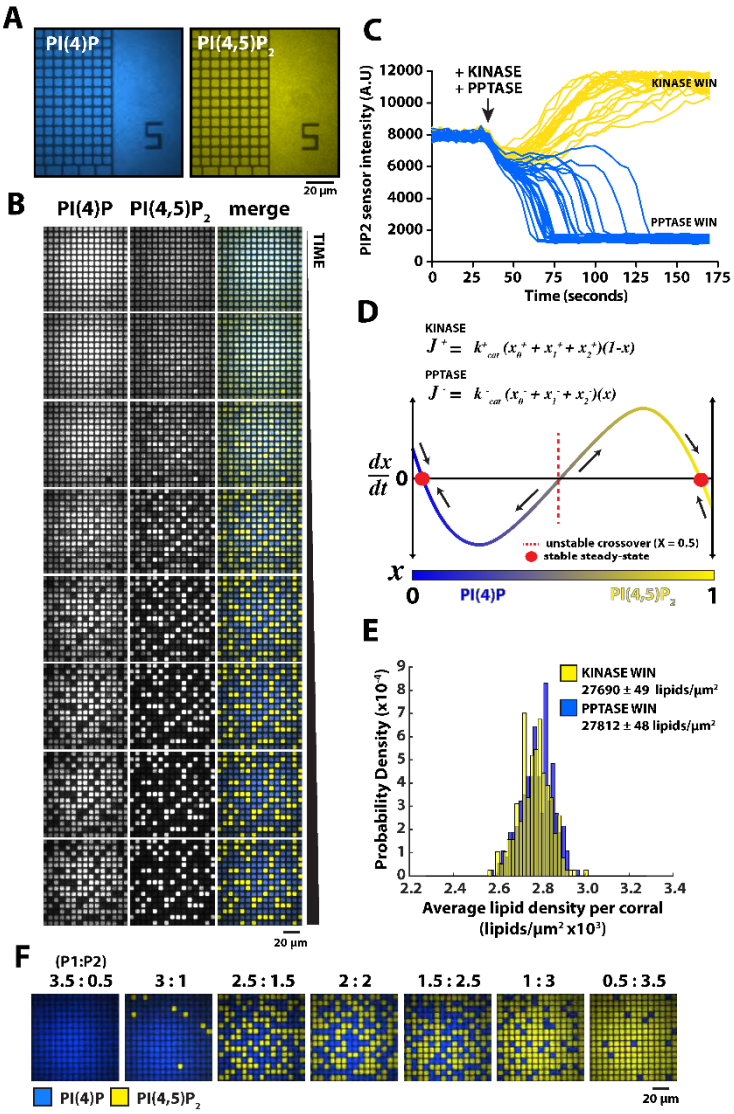

Fig. 7-2 Reconstitution of a bistable kinase-phosphatase competition reaction on micropatterned SLBs (A) Localization of the 20 nM Alexa647-DrrA and 20 nM Alexa488-PLCδ on chromium patterned glass surfaces. (B) Bifurcation of kinase-phosphatase competition reaction on chromium patterned SLBs (5µm x 5µm) in the presence of 50 nM PI4P5K, 30 nM DrrA-OCRL, 20 nM Alexa488-PLCδ, and 20 nM Alexa647-DrrA. Images are separated by 30 s. (C) Reaction trajectories fluctuate toward stable steady states – predominantly PI(4)P (blue) or PI(4,5)P_2 (yellow). (D) Molecular-based rate equation formalism for the kinase-phosphatase competition reaction. Assuming $k_0^+ = k_0^-, k_1^+ x = k_1^- x, k_2^+ x^2 = k_2^- x^2$, dx/dt is smooth and symmetrical reaction landscape with two stable steady states (i.e. dx/dt = 0). Each term is dependent on 'x', the normalized extent of the reaction or fraction PI(4,5)P_2. (E) Corral to corral lipid content variation does not predict kinase-phosphatase competition reaction outcome (N=220 kinase win corrals, N=230 PPtase win corrals). (F) Outcome of kinase-phosphatase competition reaction depends on the initial molar ratio of PI(4)P and PI(4,5)P_2.

The reaction landscape modeled by the molecular rate equation predicts that the competition reaction outcome is intimately linked to the membrane density of PI lipids. Our data suggests that stochastic membrane binding of the kinase and phosphatase within individual corrals drives compositional fluctuations in PI lipids, which determines the reaction outcome. However, the reaction outcome could be predetermined based on corral to corral lipid content variation. When we mapped the reaction outcome to the initial membrane composition, however, we found no correlation (Fig. 7-2E). We conclude that the corral to corral lipid content variation is negligible and below our detection limit. However, when the competition reaction was reconstituted on membranes with a defined stoichiometric imbalance in PI(4)P and PI(4,5)P_2 lipids, the frequency of individual corrals reaching either steady state changed in a predictable manner (Fig. 7-2F). For example, reactions initiated on membranes with PI(4)P:PI(4,5)P_2 > 1, favored the phosphatase reaction, while PI(4)P:PI(4,5)P_2 < 1 favored the kinase reaction (Fig. 7-2F).

Geometry sensing based on stochastic compositional fluctuations

Classical bistable systems typically generate a partial fraction of each state. However, we observed complete switching of end product as the membrane reaction size was reduced – a phenomenon we term geometry sensing. Simultaneously reconstituting the competition reaction on free SLBs, 4μm^2 corrals, and 25μm^2 corrals side-by-side in the same chamber, demonstrated that the kinase mediated PI(4,5)P_2 synthesis reaction was more favorable in corrals (Fig. 7-3AB). In some cases, a three-sided chromium barrier was sufficient for the kinase to outcompete the phosphatase and drive the membrane composition to a predominantly PI(4,5)P_2 steady state (Fig. 7-2F).

The molecular rate equation (Fig. 7-2D) predicts that an imbalance in the positive feedback strength between the competing reactions can generate an asymmetric response to stochastic PI lipid composition fluctuations. Compositional fluctuations can arise from differences in enzyme copy number, which create variation in reaction trajectory. Experimentally, the kinase-phosphatase competition reaction contains the features necessary to generate an asymmetric response that results in geometry sensing. First, there is an imbalance in the strength of kinase and phosphatase positive feedback loops (Fig. 7-4A). Second, the kinase-phosphatase competition reaction increases the PI lipid fluctuation spectrum (Fig. 7-4B). Third, the reaction trajectory

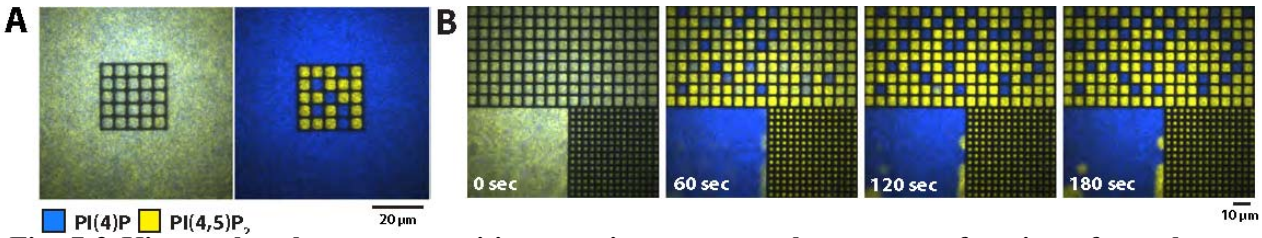

Fig. 7-3 Kinase-phosphatase competition reaction outcome changes as a function of membrane environment (A) PI4P5K displays a competitive advantage when kinase-phosphatase competition reaction is reconstituted in the presence of diffusive barriers. Images are separated by 2 min. (B) Competition reaction simultaneously reconstituted on 2μm x 2μm and 5μm x 5μm corrals side-by-side in the same chamber. For all reactions, the following protein concentrations were used: 50 nM PI4P5K, 30 nM DrrA-OCRL, 20 nM Alexa488-PLCδ, and 20 nM Alexa647-DrrA.

variation in the corral experiments is broader for the kinase compared to the phosphatase. We hypothesize that these features together enable the nonlinear reaction (i.e. kinase) to push the system to a stable steady state more frequently as the size of the reaction environment becomes smaller.

To investigate the connection between composition fluctuations and geometry sensing, we implemented a stochastic simulation with enzyme copy number as the stochastic component. We modeled the nonlinear feedback of kinase based on multivalent interactions with PI(4,5)P_2 lipids, while the phosphatase was model to interact with a single lipid species (Fig. 7-4C). In all simulations, the final reaction outcome was intimately related to the enzyme copy number and the lipid composition. The resulting stochastic simulations nicely recapitulated our experimentally measured reaction trajectories (Fig. 7-4DE). Similar to our experimental system, we simulated the kinase-phosphatase competition reaction on membranes containing the same initial lipid

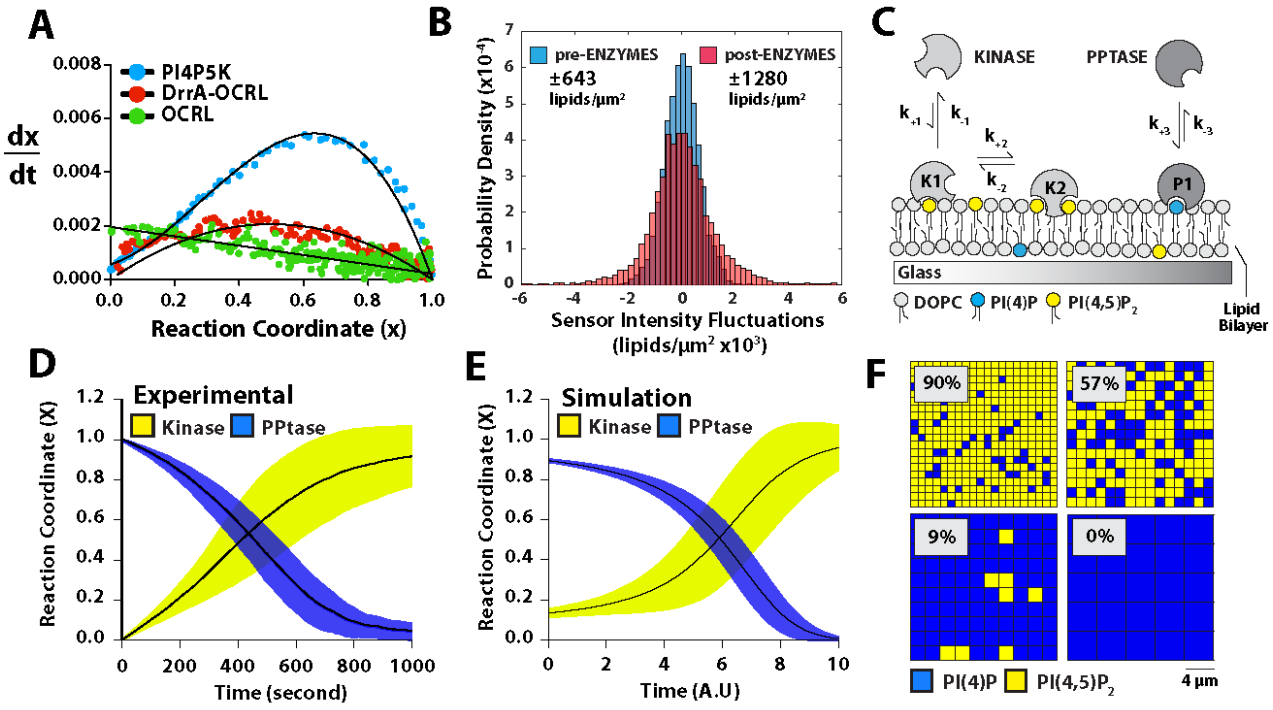

Fig. 7-4 Geometry sensing based on stochastic compositional fluctuations (A) Lipid modifying enzymes catalyze PtdIns lipid synthesis reactions with either zero, first, or second order kinetics. The normalized extent of the reaction (x) is plotted against the derivative of reaction trajectory (dx/dt) measured in the presence of 1nM PI4P5K, 10pM DrrA-OCRL, or 10nM OCRL. (B) Lipid sensor fluctuation spectrum measured in the presence of 20 nM Alexa488-PLCδ before and after the addition of kinase-phosphatase competition reaction – 10 nM PI4P5K and 5 nM DrrA-OCRL (N=256 corrals). Fluctuation measurements were limited to times before bifurcation of reaction trajectories. (C) Model for depicting kinase and phosphatase membrane binding. (D) Average corral reaction trajectory measured in the presence of 2.5 nM PI4P5K (yellow) or 10 pM DrrA-OCRL (blue) alone (n = 256 corrals, highlighted bars represent SD). (E) Average kinase and phosphatase reaction trajectory from simulation. (F) Stochastic simulation of kinase-phosphatase competition reaction recapitulates geometry sensing.

composition, but different size. Like our experiments, we observed complete switching of product as the reaction environment changed size (Fig. 7-4F).

What are the minimal requirements for the emergent property of geometry sensing? Intuitively, fluctuations vary in magnitude relative to the size of the reaction environment. As a result, the final outcome of the competition reaction can be modulated by the membrane size. Both chemical kinetic analysis and stochastic simulations indicate that a competition reaction of this nature must fulfill at least two requirements in order to exhibit geometry sensing: (1) the presence of nonlinear kinetics that are at least second order and (2) the competing reactions must have catalytic rates of similar magnitude at the unstable steady-state. The later one is experimentally realized by balancing the competitive reactions, while the nonlinear kinetics of the kinase stem from the multivalent interaction with $PI(4,5)P_2$ lipids. Broadly speaking, these requirements are fulfilled by many cellular signaling reactions, including other kinase-phosphatase systems. These include competition between GTPase activating proteins (GAPs) and guanine nucleotide exchange factors (GEFs) that control the activation of GTPases such as Ras (23, 94, 95). Considering the emergent property of geometry sensing, the extent of protein phosphorylation or nucleotide state in many futile biochemical reactions is predicted to be strongly influenced by stochastic compositional fluctuations that are coupled to geometric changes in the reaction environment.

Appendix: Details on enzyme kinetics modeling

For reactions with only the presence of kinase or phosphatase, the evolution of membrane composition can be described by either: (1) bimolecular reaction, (2) simple feedback kinetics or, (3) higher order feedback kinetics. The routine to determine the type of kinetics begins with evaluating whether the first derivative of the composition trace has a local maximum. Existence of local maximum suggests that it is a feedback reaction, otherwise it is a bimolecular reaction. For feedback reactions, it is regarded as a simple type if the kinetic traces can be fit with Eq. 7.2. Otherwise, it is regarded as a higher order feedback reaction, in which for example complex oligomerization may take place. In the following we describe the bimolecular and simple feedback reaction with the example of phosphorylation of PIP_1 lipids.

Bimolecular reaction Low concentration of kinase in solution phosphorylating PIP_1 lipids (i.e. PI(4)P) on membrane surfaces follows this type of reaction:

$$x_{kinase} + x_{PIP_1} \xrightarrow{k_2} x_{kinase} + x_{PIP_2}$$

where x_i denotes the concentration or density of the *i* component, and k_i denotes the rate constants. For $x_{PIP_2}(t=0) = \frac{N}{2}$, $x_{PIP_2}(t) = N(1 - \frac{1}{2}e^{-kt})$, where N is the total density of PIP lipids, and $k = k_2\,[A]$.

Simple feedback reaction Phosphorylation of PIP_1 lipids from PIP_2-recruited kinase from solution can be described by a simple feedback reaction:

$$x_{kinase} + x_{PIP_2} \underset{k-1}{\overset{k1}{\rightleftarrows}} x_{PIP_2:kinase} + x_{PIP_1} \xrightarrow{k_2} x_{PIP_2:kinase} + x_{PIP_2}$$

By assuming that the recruitment kinetics to be much faster than the catalysis step, the rate law for the simple feedback mechanism is:

$$\frac{dx_{PIP_2}}{dt} = k_2 x_{PIP_2:kinase} x_{PIP_1} = a x_{PIP_2} x_{PIP_1} = a x_{PIP_2}(N - x_{PIP_2})$$

where $a = k_2 \frac{k_1}{k_{-1}}[kinase]$. This differential equation is known as Bernoulli equation, and can be solved with the initial condition $x_{PIP_2}(0) = \frac{N}{2}$:

$$x_{PIP_2}(t) = \frac{N}{1+e^{-aNt}} \quad [7.2]$$

Molecular rate equation

To express the kinase-phosphatase competition reaction in a single formalism that accounts for different types of enzymatic reactions, the reconstructed kinetics can be represented using the following expression:

$$\frac{dx}{dt} = J^+ - J^- \quad [7.3]$$

$$J^+ = k_{cat}^+(x_0^+ + x_1^+ + x_2^+ + \cdots)(1 - x), \quad J^- = k_{cat}^-(x_0^- + x_1^- + x_2^- + \cdots)x \quad [7.4]$$

where $x = \frac{x_{PIP_2}}{x_{PIP_1}+x_{PIP_2}}$ denotes the normalized extent of the reaction defined by the density of PIP_1 and PIP_2 on membranes, J^+ and J^- describes the forward and reverse chemical flux, k_{cat} denotes the effective catalytic parameter and $\{x_0, x_1, x_2\}$ corresponds to the densities of each molecular species exhibiting bimolecular, simple feedback and complex feedback, respectively. Note that the subscript *i* in x_i denotes the order of dependence on *x*. This expression provides a general formalism for any chemical reaction(s) that do not follow simple Michaelian kinetics. Since all enzymatic kinetics described above can be effective represented by this expression, this formalism was used for the stochastic simulations. The bimolecular and simple feedback reaction can be mapped to the zero and the first order term in the molecular rate equation, respectively: $\frac{dx}{dt} = k_2(1 - x)$, $\frac{dx}{dt} = aN(1 - x)x$ where k_2, *a* and *N* are the same as defined previously. Higher order feedback kinetics can be represented by higher order terms. In practice, a second order term was shown to be sufficient in representing the higher order feedback kinetics in the reconstitution experiments.

Stochastic Simulations

To simulate bistable reactions in small corrals, the membrane composition within a corral was approximated as homogeneous. Since the stochastic fluctuation arise from enzyme recruitment, enzyme copy number were simulated stochastically using the Gillespie algorithm (96). Catalysis (which are highly processive on membranes) were treated as deterministic, calculated by the chemical flux described by the molecular rate equation: $\frac{dx}{dt} = J^+ + J^-$. We used rate parameters

relevant to the reconstitution experiments. For simulation capable of performing geometry sensing, the rate parameters are: $k_1 = k_5 = 0.002, k_2 = \frac{0.0004}{l^2}, k_3 = 10, k_4 = k_6 = 1, k_{cat}^{+} = k_{cat}^{-} = \frac{0.00001}{l^2}$ where *l* is the side of a squared membrane patch. Each molecular species are expressed as the number of molecule such that both unimolecular and bimolecular kinetics are expressed as the probability of the reaction when multiplied by time. For the case where both the kinase and phosphatase has simple feedback, the rate parameters are: $k_1 = k_5 = 0.002, k_3 = 0.95, k_6 = 1, k_{cat}^{+} = k_{cat}^{-} = \frac{0.00001}{l^2}$ with all other $k_i = 0$. All simulations begin with $x = 0.5$ and all enzymes in solution.

8. Final Remarks

So far, we have broken down activation of cytosolic proteins in membrane signaling reactions into recruitment and catalysis. We described how membrane recruitment are embedded with kinetic proofreading, how cells can modulate this mechanism via multivalent molecular assembly, how catalysis after successful recruitment takes place on membranes, and how a competitive network based on recruited enzymes forming different molecular configurations give rise to geometry sensing. The gradual connection to cellular complexity is the emerging direction of which worth pursuing. Rather than building complexity of the *in vitro* reconstitution, the main purpose of these experiments is to provide conceptualization in a well-controlled model system, therefore motivating specific cellular experiments to examine the physiological relevance. For example, a framework reconciling the single-molecule SOS activation timescale with cellular timescale is a topic worth delving into – the discrepancy between the long (~ 50 sec) activation time of SOS and cellular activation time (< 3 min), a problem I termed activation timescale paradox, requires further development of a framework evaluating the role of protein copy number on response time. Discussion as such hints at the design principle behind how cells function. The current biochemical-reconstitution and cellular techniques, single-molecule imaging technology, theoretical and analytical foundation are mature to scrutinize the physical principles of signal transduction. Frameworks that connect molecular processes to cellular network response is particularly paramount at this stage, and should be the main focus of recent endeavor.

Reference

1. Houtman JCD*, et al.* (2006) Oligomerization of signaling complexes by the multipoint binding of GRB2 to both LAT and SOS1. *Nat Struct Mol Biol* 13(9):798-805.
2. Groves JT & Kuriyan J (2010) Molecular mechanisms in signal transduction at the membrane. *Nat Struct Mol Biol* 17(6):659-665.
3. Dustin ML & Groves JT (2012) Receptor Signaling Clusters in the Immune Synapse. *Annu Rev Biophys* 41:543-556.
4. Chakraborty AK & Weiss A (2014) Insights into the initiation of TCR signaling. *Nat Immunol* 15(9):798-807.
5. Abraham RT & Weiss A (2004) Timeline - Jurkat T cells and development of the T-cell receptor signalling paradigm. *Nat Rev Immunol* 4(4):301-308.
6. O'Donoghue GP, Pielak RM, Smoligovets AA, Lin JJ, & Groves JT (2013) Direct single molecule measurement of TCR triggering by agonist pMHC in living primary T cells. *eLife* 2:e00778.
7. Samelson LE (2002) Signal transduction mediated by the T cell antigen receptor: The role of adapter proteins. *Annu Rev Immunol* 20:371-394.
8. Zikherman J & Au-Yeung B (2015) The role of T cell receptor signaling thresholds in guiding T cell fate decisions. *Curr Opin Immunol* 33C:43-48.
9. Goldstein B, Faeder JR, & Hlavacek WS (2004) Mathematical and computational models of immune-receptor signalling. *Nat Rev Immunol* 4(6):445-456.
10. Scott JD & Pawson T (2009) Cell Signaling in Space and Time: Where Proteins Come Together and When They're Apart. *Science* 326(5957):1220-1224.
11. Gureasko J*, et al.* (2008) Membrane-dependent signal integration by the Ras activator Son of sevenless. *Nat Struct Mol Biol* 15(6):651-651.
12. Gureasko J*, et al.* (2010) Role of the histone domain in the autoinhibition and activation of the Ras activator Son of Sevenless. *Proc Natl Acad Sci USA* 107(8):3430-3435.
13. Huang WYC*, et al.* (2016) Phosphotyrosine-mediated LAT assembly on membranes drives kinetic bifurcation in recruitment dynamics of the Ras activator SOS. *Proc Natl Acad Sci USA* 113(29):8218-8223.
14. Hopfield JJ (1974) Kinetic proofreading - new mechanism for reducing errors in biosynthetic processes requiring high specificity. *Proc Natl Acad Sci USA* 71(10):4135-4139.
15. Ozbudak EM, Thattai M, Kurtser I, Grossman AD, & van Oudenaarden A (2002) Regulation of noise in the expression of a single gene. *Nat Genet* 31(1):69-73.
16. Moffitt JR, Chemla YR, & Bustamante C (2010) Methods in statistical kinetics. *Methods Enzymol*, ed Walter NG (Elsevier Academic Press Inc, San Diego), Vol 475, pp 221-257.
17. Kou SC, Cherayil BJ, Min W, English BP, & Xie XS (2005) Single-molecule Michaelis-Menten equations. *J Phys Chem B* 109(41):19068-19081.
18. Cai L, Friedman N, & Xie XS (2006) Stochastic protein expression in individual cells at the single molecule level. *Nature* 440(7082):358-362.
19. Lu HP, Xun LY, & Xie XS (1998) Single-molecule enzymatic dynamics. *Science* 282(5395):1877-1882.
20. Christensen SM*, et al.* (2016) One-way membrane trafficking of SOS in receptor-triggered Ras activation. *Nat Struct Mol Biol* 23(9):838-846.
21. Sastry L*, et al.* (1995) Quantitative-Analysis of Grb2-Sos1 Interaction - the N-Terminal Sh3 Domain of Grb2 Mediates Affinity. *Oncogene* 11(6):1107-1112.

22. Houtman JCD*, et al.* (2004) Binding specificity of multiprotein signaling complexes is determined by both cooperative interactions and affinity preference. *Biochemistry* 43(14):4170-4178.
23. Iversen L*, et al.* (2014) Ras activation by SOS: Allosteric regulation by altered fluctuation dynamics. *Science* 345(6192):50-54.
24. Nye JA & Groves JT (2008) Kinetic control of histidine-tagged protein surface density on supported lipid bilayers. *Langmuir* 24(8):4145-4149.
25. Lin WC*, et al.* (2014) H-Ras forms dimers on membrane surfaces via a protein-protein interface. *Proc Natl Acad Sci USA* 111(8):2996-3001.
26. Groves JT, Ulman N, & Boxer SG (1997) Micropatterning fluid lipid bilayers on solid supports. *Science* 275(5300):651-653.
27. Rohatgi R, Ho HYH, & Kirschner MW (2000) Mechanism of N-WASP activation by CDC42 and phosphatidylinositol 4,5-bisphosphate. *J Cell Biol* 150(6):1299-1309.
28. Wang Q*, et al.* (2015) Autoinhibition of Bruton's tyrosine kinase (Btk) and activation by soluble inositol hexakisphosphate. *eLife* 4:e06074.
29. Schlessinger J (2000) Cell signaling by receptor tyrosine kinases. *Cell* 103(2):211-225.
30. Banjade S & Rosen MK (2014) Phase Transitions of Multivalent Proteins Can Promote Clustering of Membrane Receptors. *eLife* 3:e04123.
31. Janes PW, Nievergall E, & Lackmann M (2012) Concepts and consequences of Eph receptor clustering. *Semin Cell Dev Biol* 23(1):43-50.
32. Lisabeth EM, Falivelli G, & Pasquale EB (2013) Eph Receptor Signaling and Ephrins. *Cold Spring Harbor Perspectives in Biology* 5(9).
33. Salaita K*, et al.* (2010) Restriction of Receptor Movement Alters Cellular Response: Physical Force Sensing by EphA2. *Science* 327(5971):1380-1385.
34. Lohmuller T, Xu Q, & Groves JT (2013) Nanoscale Obstacle Arrays Frustrate Transport of EphA2-Ephrin-A1 Clusters in Cancer Cell Lines. *Nano Lett* 13(7):3059-3064.
35. Greene AC*, et al.* (2014) Spatial Organization of EphA2 at the Cell-Cell Interface Modulates Trans-Endocytosis of EphrinA1. *Biophys J* 106(10):2196-2205.
36. Lillemeier BF*, et al.* (2010) TCR and Lat are expressed on separate protein islands on T cell membranes and concatenate during activation. *Nat Immunol* 11(6):543-543.
37. Caculitan NG*, et al.* (2014) Size-based chromatography of signaling clusters in a living cell membrane. *Nano Lett* 14(5):2293-2298.
38. Lowenstein EJ*, et al.* (1992) The Sh2 and Sh3 Domain Containing Protein Grb2 Links Receptor Tyrosine Kinases to Ras Signaling. *Cell* 70(3):431-442.
39. Nag A, Monine MI, Faeder JR, & Goldstein B (2009) Aggregation of Membrane Proteins by Cytosolic Cross-Linkers: Theory and Simulation of the LAT-Grb2-SOS1 System. *Biophys J* 96(7):2604-2623.
40. Kortum RL*, et al.* (2013) The Ability of Sos1 to Oligomerize the Adaptor Protein LAT Is Separable from Its Guanine Nucleotide Exchange Activity in Vivo. *Science Signaling* 6(301):ra99.
41. Balagopalan L, Kortum RL, Coussens NP, Barr VA, & Samelson LE (2015) The Linker for Activation of T Cells (LAT) Signaling Hub: From Signaling Complexes to Microclusters. *J Biol Chem* 290(44):26422-26429.
42. Li P*, et al.* (2012) Phase transitions in the assembly of multivalent signalling proteins. *Nature* 483(7389):336-U129.

43. Douglass AD & Vale RD (2005) Single-molecule microscopy reveals plasma membrane microdomains created by protein-protein networks that exclude or trap signaling molecules in T cells. *Cell* 121(6):937-950.
44. Zhu M, Janssen E, & Zhang W (2003) Minimal requirement of tyrosine residues of linker for activation of T cells in TCR signaling and thymocyte development. *J Immunol* 170(1):325-333.
45. Lin J & Weiss A (2001) Identification of the minimal tyrosine residues required for linker for activation of T cell function. *J Biol Chem* 276(31):29588-29595.
46. Oh D*, et al.* (2012) Fast rebinding increases dwell time of Src homology 2 (SH2)-containing proteins near the plasma membrane. *Proc Natl Acad Sci USA* 109(35):14024-14029.
47. McKeithan TW (1995) Kinetic proofreading in T-cell receptor signal transduction. *Proc Natl Acad Sci USA* 92(11):5042-5046.
48. Paz PE*, et al.* (2001) Mapping the Zap-70 phosphorylation sites on LAT (linker for activation of T cells) required for recruitment and activation of signalling proteins in T cells. *Biochem J* 356:461-471.
49. Rubinstein M & Colby RH (2003) *Polymer Physics* (Oxford University Press, New York, U.S.A.).
50. Ensign DL & Pande VS (2010) Bayesian Detection of Intensity Changes in Single Molecule and Molecular Dynamics Trajectories. *J Phys Chem B* 114(1):280-292.
51. Chook YM, Gish GD, Kay CM, Pai EF, & Pawson T (1996) The Grb2-mSos1 complex binds phosphopeptides with higher affinity than Grb2. *J Biol Chem* 271(48):30472-30478.
52. Christensen ST, Meredith; Rhodes, Christopher; Iwig, Jeffrey; Tu, Hsiung-Lin; Stamou, Dimitrios; Groves, Jay (2016) Monitoring the waiting time sequence of single Ras GTPase activation events using liposome functionalized zero mode waveguides. *Nano Lett* 16(4):2890–2895.
53. Bezanilla F (2005) Voltage-gated ion channels. *IEEE Trans NanoBiosci* 4(1):34-48.
54. Das J*, et al.* (2009) Digital Signaling and Hysteresis Characterize Ras Activation in Lymphoid Cells. *Cell* 136(2):337-351.
55. Su XL*, et al.* (2016) Phase separation of signaling molecules promotes T cell receptor signal transduction. *Science* 352(6285):595-599.
56. Flory PJ (1941) Molecular size distribution in three dimensional polymers. I. Gelation. *J Am Chem Soc* 63:3083-3090.
57. Hyman AA & Simons K (2012) Beyond Oil and Water-Phase Transitions in Cells. *Science* 337(6098):1047-1049.
58. Groves JT, Parthasarathy R, & Forstner MB (2008) Fluorescence imaging of membrane dynamics. *Annu Rev Biomed Eng* 10:311-338.
59. Rozovsky S, Forstner MB, Sondermann H, & Groves JT (2012) Single Molecule Kinetics of ENTH Binding to Lipid Membranes. *J Phys Chem B* 116(17):5122-5131.
60. Chung JK, Lee YK, Lam HYM, & Groves JT (2016) Covalent Ras Dimerization on Membrane Surfaces through Photosensitized Oxidation. *J Am Chem Soc* 138(6):1800-1803.
61. Verdier PH & Stockmayer WH (1962) Monte Carlo Calculations on Dynamics of Polymers in Dilute Solution. *J Chem Phys* 36(1):227-+.
62. Baumgartner A (1984) Simulation of Polymer Motion. *Annu Rev Phys Chem* 35:419-435.
63. Izeddin I*, et al.* (2014) Single-molecule tracking in live cells reveals distinct target-search strategies of transcription factors in the nucleus. *eLife* 3:e02230.

64. Condamin S, Tejedor V, Voituriez R, Benichou O, & Klafter J (2008) Probing microscopic origins of confined subdiffusion by first-passage observables. *Proc Natl Acad Sci USA* 105(15):5675-5680.
65. Dix JA & Verkman AS (2008) Crowding effects on diffusion in solutions and cells. *Annu Rev Biophys* 37:247-263.
66. Rouse PE (1953) A Theory of the Linear Viscoelastic Properties of Dilute Solutions of Coiling Polymers. *J Chem Phys* 21(7):1272-1280.
67. Degennes PG (1971) Reptation of a Polymer Chain in Presence of Fixed Obstacles. *J Chem Phys* 55(2):572-&.
68. Sako Y & Kusumi A (1994) Compartmentalized structure of the plasma membrane for receptor movements as revealed by a nanometer-level motion analysis. *J Cell Biol* 125(6):1251-1264.
69. Good MC, Zalatan JG, & Lim WA (2011) Scaffold Proteins: Hubs for Controlling the Flow of Cellular Information. *Science* 332(6030):680-686.
70. Huang J*, et al.* (2010) The kinetics of two-dimensional TCR and pMHC interactions determine T-cell responsiveness. *Nature* 464(7290):932-U156.
71. Huppa JB*, et al.* (2010) TCR-peptide-MHC interactions in situ show accelerated kinetics and increased affinity. *Nature* 463(7283):963-U143.
72. Patwardhan P & Miller WT (2007) Processive phosphorylation: mechanism and biological importance. *Cell Signal* 19(11):2218-2226.
73. Gopich IV & Szabo A (2013) Diffusion modifies the connectivity of kinetic schemes for multisite binding and catalysis. *Proc Natl Acad Sci USA* 110(49):19784-19789.
74. Pawson T, Gish GD, & Nash P (2001) SH2 domains, interaction modules and cellular wiring. *Trends Cell Biol* 11(12):504-511.
75. Herrmann C, Martin GA, & Wittinghofer A (1995) Quantitative-Analysis of the Complex between P21(Ras) and the Ras-Binding Domain of the Human Raf-1 Protein-Kinase. *J Biol Chem* 270(7):2901-2905.
76. Botelho RJ*, et al.* (2000) Localized biphasic changes in phosphatidylinositol-4,5-bisphosphate at sites of phagocytosis. *J Cell Biol* 151(7):1353-1368.
77. Scott CC*, et al.* (2005) Phosphatidylinositol-4,5-bisphosphate hydrolysis directs actin remodeling during phagocytosis. *J Cell Biol* 169(1):139-149.
78. Arai Y*, et al.* (2010) Self-organization of the phosphatidylinositol lipids signaling system for random cell migration. *Proc Natl Acad Sci U S A* 107(27):12399-12404.
79. Lacalle RA*, et al.* (2015) Type I phosphatidylinositol 4-phosphate 5-kinase homo- and heterodimerization determines its membrane localization and activity. *FASEB J* 29(6):2371-2385.
80. Jin H, McCaffery JM, & Grote E (2008) Ergosterol promotes pheromone signaling and plasma membrane fusion in mating yeast. *J Cell Biol* 180(4):813-826.
81. Garrenton LS, Stefan CJ, McMurray MA, Emr SD, & Thorner J (2010) Pheromone-induced anisotropy in yeast plasma membrane phosphatidylinositol-4,5-bisphosphate distribution is required for MAPK signaling. *Proc Natl Acad Sci U S A* 107(26):11805-11810.
82. Shi XS*, et al.* (2013) Ca2+ regulates T-cell receptor activation by modulating the charge property of lipids. *Nature* 493(7430):111-+.
83. Gierer A & Meinhardt H (1972) A theory of biological pattern formation. *Kybernetik* 12(1):30-39.

84. Meinhardt H (1982) *Models of biological pattern formation* (Academic Press, London) pp xi,230p.
85. Turing AM (1990) The chemical basis of morphogenesis. 1953. *Bull Math Biol* 52(1-2):153-197; discussion 119-152.
86. Groves JT & Boxer SG (2002) Micropattern formation in supported lipid membranes. *Accounts of Chemical Research* 35(3):149-157.
87. Baksh MM, Jaros M, & Groves JT (2004) Detection of molecular interactions at membrane surfaces through colloid phase transitions. *Nature* 427(6970):139-141.
88. Rameh LE, Tolias KF, Duckworth BC, & Cantley LC (1997) A new pathway for synthesis of phosphatidylinositol-4,5-bisphosphate. *Nature* 390(6656):192-196.
89. Pirruccello M & De Camilli P (2012) Inositol 5-phosphatases: insights from the Lowe syndrome protein OCRL. *Trends Biochem Sci* 37(4):134-143.
90. Ragaz C*, et al.* (2008) The Legionella pneumophila phosphatidylinositol-4 phosphate-binding type IV substrate SidC recruits endoplasmic reticulum vesicles to a replication-permissive vacuole. *Cell Microbiol* 10(12):2416-2433.
91. Brombacher E*, et al.* (2009) Rab1 guanine nucleotide exchange factor SidM is a major phosphatidylinositol 4-phosphate-binding effector protein of Legionella pneumophila. *J Biol Chem* 284(8):4846-4856.
92. Schoebel S, Blankenfeldt W, Goody RS, & Itzen A (2010) High-affinity binding of phosphatidylinositol 4-phosphate by Legionella pneumophila DrrA. *EMBO Rep* 11(8):598-604.
93. Lemmon MA, Ferguson KM, O'Brien R, Sigler PB, & Schlessinger J (1995) Specific and high-affinity binding of inositol phosphates to an isolated pleckstrin homology domain. *Proc Natl Acad Sci U S A* 92(23):10472-10476.
94. Christensen SM*, et al.* (2016) Monitoring the Waiting Time Sequence of Single Ras GTPase Activation Events Using Liposome Functionalized Zero-Mode Waveguides. *Nano Lett* 16(4):2890-2895.
95. Margarit SM*, et al.* (2003) Structural evidence for feedback activation by Ras.GTP of the Ras-specific nucleotide exchange factor SOS. *Cell* 112(5):685-695.
96. Gillespie DT (1976) A general method for numerically simulating the stochastic time evolution of coupled chemical reactions. *J Comput Phys* 22(4):403-434.